NASA TM X-55540

A CHAIN MATRIX ANALYSIS
OF AN ELECTRONIC BORESIGHT
SCANNING TECHNIQUE FOR A
DUAL-PLANE AMPLITUDE-SENSING
MONOPULSE ANTENNA

19 JULY 1965

GODDARD SPACE FLIGHT CENTER
GREENBELT, MARYLAND

N66 30363

(ACCESSION NUMBER)	(THRU)
59	1
(PAGES)	(CODE)
TMX-55540	02
(NASA CR OR TMX OR AD NUMBER)	(CATEGORY)

FACILITY FORM 602

A CHAIN MATRIX ANALYSIS OF
AN ELECTRONIC BORESIGHT SCANNING TECHNIQUE
FOR A DUAL-PLANE AMPLITUDE-SENSING
MONOPULSE ANTENNA

by

Armondo D. Elia

and

Richard F. Schmidt

19 July 1965

GODDARD SPACE FLIGHT CENTER

Greenbelt, Maryland

ABSTRACT

30363

This report is an analysis of a dual-plane amplitude-sensing mono-pulse system which relates to the essentially inertialess displacement of the sum and difference patterns in space with respect to the antenna coordinates. The development is predicated on the concept of scattering and transfer matrices. It is shown that the dual-plane electronic boresight scanning (EBS) problem considered here can be regarded as lying in an eight-dimensional vector space in which the terminal quantities are analogous to the basis vectors which span the space. The transmission and reception properties of the circuit are separated by a direct-sum decomposition and only the reception case is considered in detail for the angular resolution problem treated herein. This is an interim report pertaining to the formulation of the problem and does not treat any particular physical situation or present graphs of the output channel signals. A second report has been initiated for this purpose.

CONTENTS

A CHAIN MATRIX ANALYSIS OF AN ELECTRONIC BORESIGHT SCANNING TECHNIQUE FOR A DUAL-PLANE AMPLITUDE-SENSING MONOPULSE ANTENNA

INTRODUCTION

The primary objective of a monopulse data-acquisition antenna is to provide a maximum gain in the data channel by pointing the peak of the sum pattern accurately in the direction of arrival of the telemetry signal. This is accomplished by positioning the antenna so as to null the difference signal. When the RF system is properly aligned, the difference signal null coincides with the maximum of the sum signal and with the mechanical center line of the parabola. Proper alignment is important since the servo-control system senses only the difference-pattern null and assumes that the sum-pattern maximum is coincident.

The purpose of the work reported here is to provide a means of separating the problem of directing the RF boresight accurately and rapidly from the problem of mechanically moving the antenna structure. The proposed technique requires the development of a method of scanning the sum-and-difference patterns (preferably electronically) throughout a small cone centered on the mechanical center line of the dish. An equivalent effect may be achieved by operating on the signals from the RF feeds to simulate a motion of the boresight. This boresight control is referred to as Electronic Boresight Scanning (EBS). Given such a control, a conventional servo system, having reduced accuracy and response requirements, could be used to move the antenna structure to keep the line of sight to the spacecraft within the EBS cone. The mechanical system would follow the spacecraft with moderate accuracy while the EBS system produced a correcting vernier motion (real or simulated) of the boresight relative to the mechanical center line. A brief discussion of the antenna servo-control problem will indicate the main basis for interest in the proposed system.

A major restriction in the design of the servo-control system is produced by the mechanical resonances associated with the antenna structure, gearing, and drive. Typically, the lowest frequency resonances and, therefore, those of most concern, occur at two to three cycles per second in 85-foot antennas and produce resonant rises of 6 to 18 decibels (db). Both the damping and the frequency of the resonance may be expected to change with antenna orientation, wind loading, etc. Adaptive techniques to track and suppress resonances are being investigated. Lacking such advanced and complex systems, however, stability requirements dictate that the servo bandwidth be limited to frequencies substantially below the

1

resonant frequency. Figure 1 gives the open-loop frequency response (Bode plot) of a typical Type II system having a resonant peak due to the load. For a satisfactory transient response, it is necessary that the peak be not less than 6 db below the 0 db gain level. The geometry of the plot determines the maximum obtainable cross-over frequency, F_c, which is a close approximation to the closed-loop bandwidth. F_c is normally less than one cycle per second in 85-foot antennas and may be 0.4 cycles per second or less. The shaded area indicates the frequencies to which the servo system must respond in following a satellite and correcting for disturbances. A low value of F_c limits the gain at these frequencies and, therefore, increases the error resulting from satellite track dynamics. To a lesser extent, errors caused by wind gusts and mechanical systems friction torque variations are also increased.
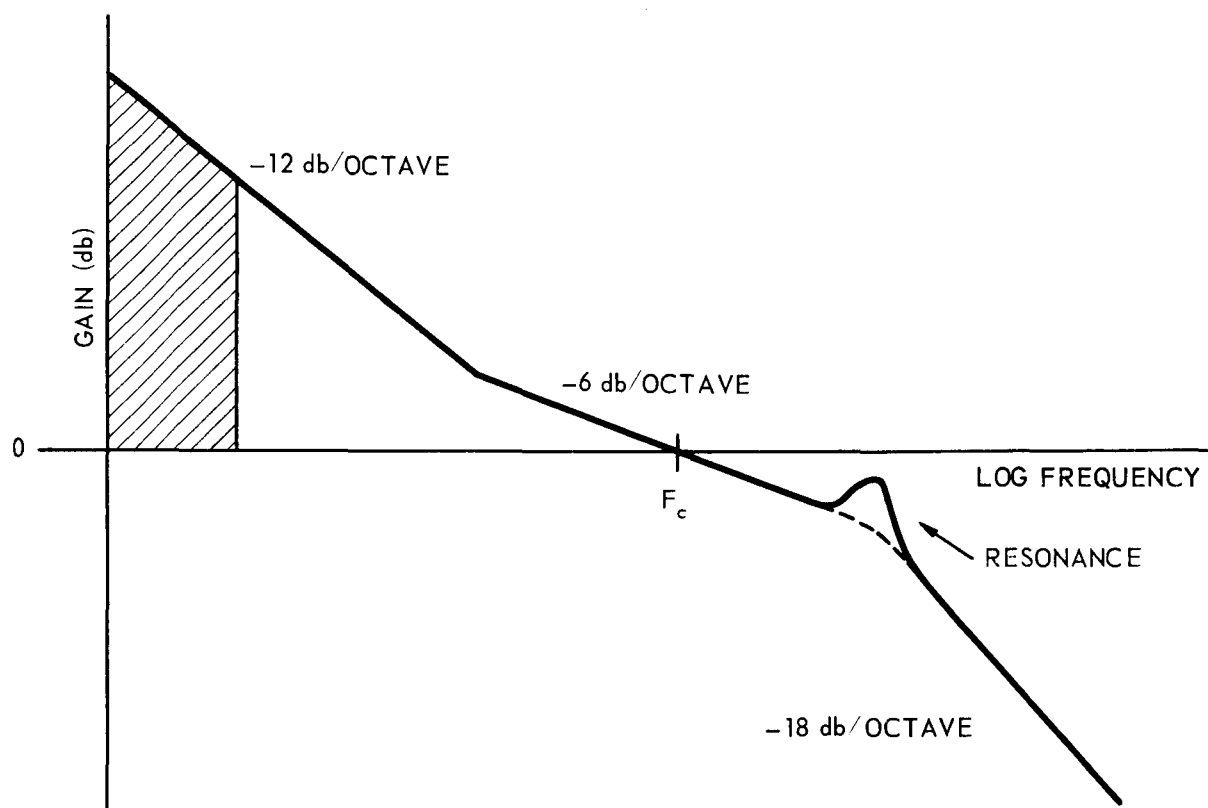

Figure 1—Bode Diagram

Additional design restrictions are imposed by stiction in the gears, bearings, and hydraulic-drive subsystem, particularly the servo values; drive-motor speed range, maximum torque, and torque ripple; and other drive and load non-linearities. These undesirable characteristics increase dead zone and degrade low-speed performance.

2

As a result of the restrictions listed, servo-control systems designed for the accuracy and transient response necessary in space data-acquisition antennas are complex and demand high levels of performance from critically adjusted components. This leads to systems which require frequent retuning and which inherently have less than the desired reliability. The proposed system is intended to relieve this situation by permitting a relaxation in the servo-control system specifications. Simultaneously, improved pointing accuracy and low-speed performance appear possible.

One configuration of the EBS servo-control system is given in Figure 2. As has been stated, equivalent results, as far as the control system is concerned, could be obtained by actually scanning the sum and difference patterns about the mechanical center line of the dish or by operating on the signals from the feeds to give an apparent scanning effect. Figure 2 is based upon the latter concept. The system consists of two loops which are independent within limits except that the inner, EBS, loop has as its reference, or center position, the output of the servo loop. The EBS circuit has the property of producing a certain apparent angular displacement of the boresight per unit of E' applied. The EBS loop forms an accurate, fast-response, electronic-control system in which the boresight error, E, may be made to approach zero while the boresight scanning signal, E', remains as a measure of the misalignment of the center line of the dish and the line of sight. The boresight scanning signal is applied also to the servo-loop controller where additional compensation, required by the mechanical servo, is accomplished. The servo loop positions the dish to null E'. Since the two loops seek the same null conditions and since the bandwidth (and, hence, the speed of response) of the EBS loop is made greater than that of the servo loop, there is no destructive interaction between the loops. A brief transfer-function analysis of the system and results from an analog computer simulation are given in Appendix I.
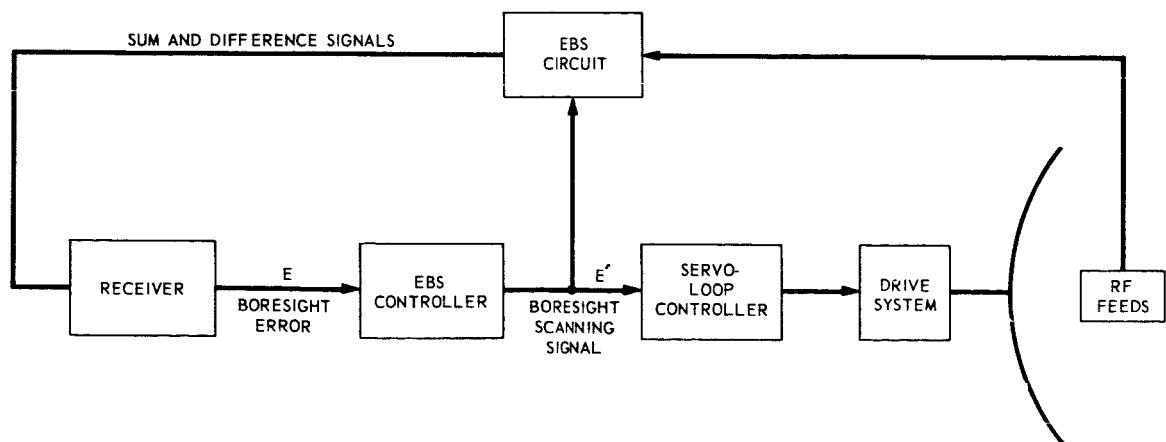
Figure 2—EBS-Servo Control System

3

Benefits which would be derived from a successful EBS development include improved low-speed performance due to the absence of mechanical stiction in the EBS loop. An essentially infinite speed range of the boresight would thus be possible. The greater bandwidth obtainable in the EBS loop would result in a reduction in the pointing error caused by target dynamics and load disturbances. In addition, step-response time would be decreased, improving acquisition capability. Error in the EBS loop due to receiver noise is increased by the greater bandwidth, but since this is normally a minor contributor to total system error, Ref. [1], a large net gain should result. Perhaps the most significant benefits would be in system reliability. The decreased gain and bandwidth permitted in the servo loop allow components to be operated more conservatively and reduce the sensitivity of system performance to changes in component characteristics. There is less excitation of structural and hydraulic-drive subsystem resonant modes and, therefore, fewer failures due to vibration and fatigue.

BACKGROUND FOR AMPLITUDE-SENSING MONOPULSE

The problem under consideration is that of accomplishing electronic boresight scanning for a dual-plane amplitude-sensing monopulse system. Specifically, this is an attempt to determine the feasibility of displacing the sum and difference patterns in space at three frequencies (136 mc, 400 mc, 1705 mc), simultaneously and independently, for the Goddard STADAN 85-foot parabolic reflector installations with

$$\frac{F\,(focal\;length)}{d\,(diameter)} = 0.424.$$

At this time, structural modification of the existing installation is precluded and a technique which necessitates a minimum amount of retrofitting is sought. The existence of the conventional secondary patterns is assumed throughout. The problem considered here is that of operating upon, or processing, the signals derived from the secondary beams in such a manner as to bring about the displacement of the sum and difference patterns. In the absence of any known method for accomplishing dual-plane electronic boresight scanning, under the given constraints, the possibility of extension of a single plane technique described by Rhodes, Ref. [2], pp. 62-68 is investigated. The radio-frequency circuit associated with the single-plane technique is shown as Fig. 3.

Quantitative results for electronic boresight scanning in the 85-foot reflector are obtainable in a straightforward manner from a mathematical model under certain idealizations. Values pertaining to absolute field patterns, error slope, and the relationship between physically realizable electronic phase shift and the pattern displacement in space at each of the three operating frequencies are derived from the mathematical analysis with suitable parametric variations.

4

Electronic boresight scanner

θ

TR

$i\Delta$

$e^{i\frac{\beta}{2}}\Sigma_s$

M

Rect → PPI

-i

i

TR

$i\Sigma$

$e^{i\beta}$

M

~

IAGC

Phase comparator → Angle

$e^{\frac{i\beta}{2}}\Delta_s$

Linear postamplifiers

Linear preamplifiers

ATR

Sweep generator → Range reference

Transmitter

(a)

Σ_s Δ_s $-\pi$ u_{ib} π u $\beta=0°$

Σ_s $-\pi$ u_{ib} π u Δ_s $\beta=30°$

Σ_s Δ_s $-\pi$ u_{ib} π u $\beta=60°$

Σ_s $-\pi$ π Δ_s u_{ib} u $\beta=90°$

(b)

$Re\,\mathcal{F}$ $-\pi$ u_{ib} π u $\beta=0°$

$Re\,\mathcal{F}$ $-\pi$ u_{ib} π u $\beta=30°$

$Re\,\mathcal{F}$ $-\pi$ u_{ib} π u $\beta=60°$

$Re\,\mathcal{F}$ π $-\pi$ u_{ib} u $\beta=90°$

(c)

β $90°$ $-\pi$ π u_{ib} $90°$

(d)

$\dfrac{\partial\,Re\,\mathcal{F}}{\partial u}$ $u=u_{ib}$ $-\pi$ π u_{ib}

(e)

Figure 3—Electronic Boresight Scanning Circuit For Single-Plane Amplitude-Sensing Monopulse Antenna

Note: The figure above is extracted from the text "Introduction to Monopulse" by D. R. Rhodes, McGraw-Hill (1959)

5

Proceeding in a systematic manner, the overall problem is separated at the outset into two parts: (1) the monopulse four-beam secondary-pattern cluster or driving function and (2) the electronic boresight scanning circuit which successively transforms the four simultaneous signals of the driving function.

The monopulse cluster of four secondary radiation patterns is developed as follows for each operating frequency. Referring once again to Reference [2], p. 35, the radiation pattern function for an aperture with cosinusoidal amplitude distribution and constant phase distribution for single-plane amplitude-sensing is given by

$$ E = \frac{\frac{\pi^2}{4} \cos u}{\frac{\pi^2}{4} - u^2} \,, \qquad u = \pi \frac{d}{\lambda} \sin \theta \qquad (1) $$

where

$$ \lim_{u \to \pi/2} \frac{\cos u}{\pi^2/4 - u^2} = \frac{1}{\pi}. $$

Here E is the field strength, d is the aperture diameter, λ is the wavelength, and θ is the spatial angle measured from the normal to the aperture. It is noted that this radiation pattern is usually associated with a linear aperture, however, for purposes of this report the pattern function given by Eq. (1) is a satisfactory representative for the physically realizable patterns obtained in practice. A detailed calculation for the radiation pattern obtained with a nearly cosinusoidal current amplitude distribution on a circular aperture is given in Appendix II, together with a graph showing the minor deviation from the assumed relationship. The variation between the two functions is very small, at least as far as the –6 db level, and differs principally in the region of the sidelobe structure. It will be shown that the effective tracking cone excludes the regions of significant deviation between these functions.

If either the function

$$ E = \frac{\frac{\pi^2}{4} \cos u}{\frac{\pi^2}{4} - u^2} $$

or $E = \Lambda_2(u)$ is assumed to represent the on-axis radiation pattern in three dimensions (i.e. if rotational symmetry is assumed to exist) then the polarization

6

problem has been ignored and an idealization has been introduced. The actual patterns obtainable in a parabolic reflector with crossed dipoles, say, have approximately the same shape as the assumed form. In fact, an additional simplification can be introduced without adverse effect here although rigor is sacrificed. It will be assumed that the secondary pattern cluster can be represented by a beam function with the form of Eq. (1), but suitably displaced in space by the beam squint angle θ_s, ref. [2] p. 46. The feeds are offset from the focal point, but lie in the focal plane, so that

$$\sin \theta_s \cong K \frac{\Delta X}{F} \tag{2}$$

where ΔX is the feed displacement, F is the focal length of the parabolic reflector, and K is the beam deviation factor, ref. [3], p. 488. The value of K is approximately equal to 0.88 here since $F/d = 0.424$. Since the feed displacement is small, $\theta_s \cong \Delta X/F$ for the present problem. Amplitude-sensing by off-focus feeds is never quite pure due to the finite separation of phase centers. The driving function will be based on the assumption of coincident phase centers, however, in the interests of simplicity.

GENERATION OF THE SECONDARY PATTERNS
   FOR THE DUAL-PLANE CASE

   The generation of the secondary pattern four-beam clusters utilizes the Eulerian angle concept of coordinate transformation; ref. [4], pp. 1-7-109, ref. [5], pp. 95-106. At each frequency, the assumed on-axis pattern is effectively rotated by the amount θ_s, about a common center and into the proper quadrant, to produce one of the patterns of the beam cluster. A tilted coordinate frame is associated with each beam pattern in each cluster and the Euler transformation is utilized to relate field intensities on a tilted space such as (r', θ', φ') to the coordinate frame (r, θ, φ) attached to the parabolic reflector. That is, four tilted spaces are related to the reflector coordinates to produce the complete four-beam cluster at a single frequency. The complete transformation, in full generality, has the following form in Cartesian coordinates

$$\bar{x}' = A\bar{x} = \begin{bmatrix} x' \\ y' \\ z' \end{bmatrix} = \begin{bmatrix} A_{11} & A_{12} & A_{13} \\ A_{21} & A_{22} & A_{23} \\ A_{31} & A_{32} & A_{33} \end{bmatrix} \begin{bmatrix} x \\ y \\ z \end{bmatrix} \tag{3}$$

7

where each element of the column matrices is converted to the corresponding spherical coordinate expression. Field intensities can be derived for the patterns of the cluster by selecting an arbitrary field point on a hypothetical unit sphere $(1, \theta, \varphi)$, evaluating the unprimed column matrix, and performing the indicated product $A\bar{x}$. Then the primed column matrix is determined, and an ordered pair (θ', φ') is found. In this manner the simultaneous cluster intensities are found for any trajectory in (θ, φ). The matrix A is different for each pattern of the beam cluster at some specified frequency so that $A \rightarrow A_i$ and

$$\bar{x}^{I} = A_1 \bar{x}$$

$$\bar{x}^{II} = A_2 \bar{x}$$

$$\bar{x}^{III} = A_3 \bar{x}$$

(4)

$$\bar{x}^{IV} = A_4 \bar{x}$$

for beams $i = 1, 2, 3,$ and 4 respectively. A complete description of the Euler transformation, a sketch showing coordinate conventions and orientation of the antenna, and a table of the Eulerian angles α, β, γ for the four-beam clusters at 136 mc, 400 mc, and 1705 mc are found in the Appendix. Determination of the primed coordinates $(\theta^{I}, \varphi^{I})$, $(\theta^{II}, \varphi^{II})$, $(\theta^{III}, \varphi^{III})$ and $(\theta^{IV}, \varphi^{IV})$ allows evaluation of the expression

$$E_i = \frac{\cos u_i}{\dfrac{\pi^2}{4} - u_i^2} \qquad \text{for} \quad = 1, 2, 3, 4$$

Since $u_i = \dfrac{\pi d}{\lambda} \sin \theta_i$, $\theta \rightarrow \theta^{I}, \theta^{II}, \theta^{III}, \theta^{IV}$.

PROPERTIES OF THE WEIGHTING CIRCUIT

The weighting circuit is fundamental to the EBS technique under consideration, therefore its properties are discussed in some detail. Consider a weighting circuit composed of the two hybrid junctions with the scattering matrix of the following form,

$$
\mathbf{S}_{ij} = \frac{1}{\sqrt{2}}
\left[
\begin{array}{cc|cc}
0 & 0 & 1 & j \\
0 & 0 & j & 1 \\
\hline
1 & j & 0 & 0 \\
j & 1 & 0 & 0
\end{array}
\right]
$$

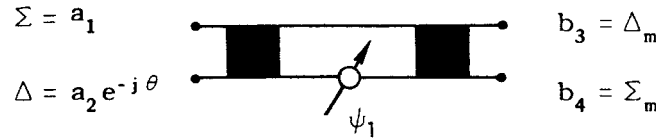and an ordinary phase shifter, connected as shown in Figure 2.

Figure 4—Weighting Circuit

Let $a_1 = \Sigma$, $a_2 e^{-j\theta} = \Delta$, represent the sum channel and error channel, respectively, in a single plane amplitude–sensing monopulse system. The time variation $e^{j\omega t}$ is factored out and $a_1 > 0$, $a_2 \geq 0$. Also $\theta = 0$ or $\theta = \pi$ only, which is consistent with the fact that the input signals from the sum and difference network are in either a cophase or antiphase relationship as the source of radiation is on one side or the other of the unscanned boresight. Since each input signal gives rise to two output signals at any output port, each of b_3 and b_4 is the complex sum of four signals. It is possible to count phase shifts and allow for power splitting in each hybrid junction to arrive at the magnitude and phase of b_3 and b_4 relative to the input quantities a_1 and $a_2 e^{-j\theta}$. A transfer matrix calculation $T_{eg.} = \mathbf{T}_{ij}\,{}_{\beta}T_{ij}\,\mathbf{T}_{ij}$ can also be employed as will be explained in detail in the section entitled TRANSFORMATIONS OF THE CHAIN MATRIX IN V_8 (c) of this report. In either case, the following results are obtained.

$$
2\,b_3 = a_1 - a_1 e^{-j\psi_1} + j\,a_2 e^{-j\theta} + j\,a_2 e^{-j\theta}\,e^{-j\psi_1}
$$

$$
2\,b_4 = j\,a_1 + j\,a_1 e^{-j\psi_1} + a_2 e^{-j\theta}\,e^{-j\psi_1} - a_2 e^{-j\theta}
$$

Using the identities $1 - \cos\psi \equiv 2\sin^2 \psi/2$, $1 + \cos\psi \equiv 2\cos^2 \psi/2$, and $\sin\psi \equiv 2\sin\psi/2\,\cos\psi/2$ it can be shown that:

$$
|b_3| = \left[a_1^2 \sin^2 \frac{\psi_1}{2} + 2a_1 a_2 \sin\frac{\psi_1}{2}\cos\frac{\psi_1}{2}\cos\theta + a_2^2 \cos^2\frac{\psi_1}{2}\right]^{1/2}
$$

$$
= \left| a_1 \sin\frac{\psi_1}{2} + a_2 \cos\frac{\psi_1}{2}\right| \quad \text{for } \theta = 0,\ a_1 > 0,\ a_2 \geq 0
$$

$$
= \left| a_1 \sin\frac{\psi_1}{2} - a_2 \cos\frac{\psi_1}{2}\right| \quad \text{for } \theta = \pi,\ a_1 > 0,\ a_2 \geq 0.
$$

9

$$|b_4| = \left[a_1^2 \cos^2 \frac{\psi_1}{2} - 2 a_1 a_2 \sin \frac{\psi_1}{2} \cos \frac{\psi_1}{2} \cos \theta + a_2^2 \sin^2 \frac{\psi_1}{2} \right]^{1/2}$$

$$= \left| a_1 \cos \frac{\psi_1}{2} - a_2 \sin \frac{\psi_1}{2} \right| \quad \text{for } \theta = 0, \ a_1 > 0, \ a_2 \geq 0$$

$$= \left| a_1 \cos \frac{\psi_1}{2} + a_2 \sin \frac{\psi_1}{2} \right| \quad \text{for } \theta = \pi, \ a_1 > 0, \ a_2 \geq 0$$

$$\tan(\arg b_3) = \frac{\cos \frac{\psi_1}{2} \left(a_1 \sin \frac{\psi_1}{2} + a_2 \cos \frac{\psi_1}{2} \right)}{\sin \frac{\psi_1}{2} \left(a_1 \sin \frac{\psi_1}{2} + a_2 \cos \frac{\psi_1}{2} \right)} \quad \text{for } \theta = 0, \ a_1 > 0, \ a_2 \geq 0$$

$$\tan(\arg b_3) = \frac{\cos \frac{\psi_1}{2} \left(a_1 \sin \frac{\psi_1}{2} - a_2 \cos \frac{\psi_1}{2} \right)}{\sin \frac{\psi_1}{2} \left(a_1 \sin \frac{\psi_1}{2} - a_2 \cos \frac{\psi_1}{2} \right)} \quad \text{for } \theta = \pi, \ a_1 > 0, \ a_2 \geq 0$$

$$\tan(\arg b_4) = \frac{\cos \frac{\psi_1}{2} \left(a_1 \cos \frac{\psi_1}{2} - a_2 \sin \frac{\psi_1}{2} \right)}{\sin \frac{\psi_1}{2} \left(a_1 \cos \frac{\psi_1}{2} - a_2 \sin \frac{\psi_1}{2} \right)} \quad \text{for } \theta = 0, \ a_1 > 0, \ a_2 \geq 0$$

$$\tan(\arg b_4) = \frac{\cos \frac{\psi_1}{2} \left(a_1 \cos \frac{\psi_1}{2} + a_2 \sin \frac{\psi_1}{2} \right)}{\sin \frac{\psi_1}{2} \left(a_1 \cos \frac{\psi_1}{2} + a_2 \sin \frac{\psi_1}{2} \right)} \quad \text{for } \theta = \pi, \ a_1 > 0, \ a_2 \geq 0$$

Cancellation of common factors in the numerator and denominator is avoided to preserve the quadrant of the phase angles $(\arg b_3)$ and $(\arg b_4)$. From the foregoing, it follows that the weighting circuit effectively introduces a phase <u>advance</u> of $(\pi - \psi_1)/2$ radians for the sum channel b_4 if $|a_1| > |a_2|$. Let $\tan \Phi = \tan(\arg b_4) = \cot(\psi_1/2) = \tan(\pi/2 - \psi_1/2)$ where $-\pi/2 \leq \psi_1 \leq \pi/2$ is the range of ψ_1. An investigation of $\tan(\arg b_3)$ shows that the difference channel information has been advanced by an equal amount Φ, to within an ambiguity of π radians since the error channel inherently possesses a plus-minus ambiguity. The phasor diagrams of Figure 5, illustrate the phase and amplitude relationships for a few cases.
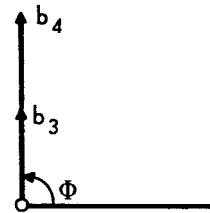
$\Sigma = a_1$ $b_3 = \Delta_m$
$\Delta = a_2$ $b_4 = \Sigma_m$
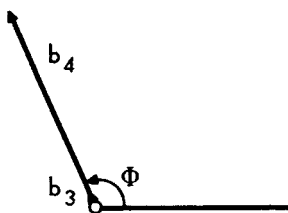ψ_1
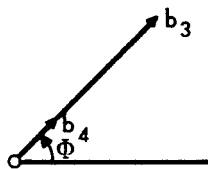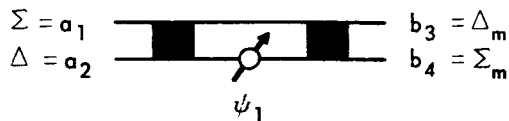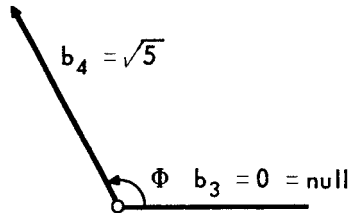
(1)
$a_1 = 2, a_2 = 1, \theta = 0°$
$\psi_1 = +90°$
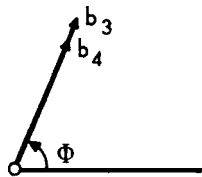
(2)
$a_1 = 2, a_2 = 1, \theta = 0°$
$\psi_1 = +45°$

(3)
$a_1 = 2, a_2 = 1, \theta = 0°$
$\psi_1 = 0°$

(4)
$a_1 = 2, a_2 = 1, \theta = 0°$
$\psi_1 = -45°$

(5) $b_4 = \sqrt{5}$, $b_3 = 0 = $ null
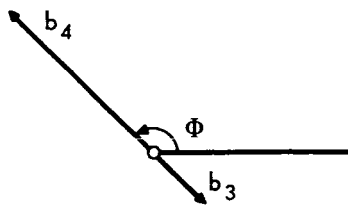$a_1 = 2, a_2 = 1, \theta = 0°$
$\psi_1 = -53.1°$
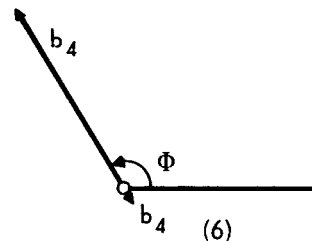
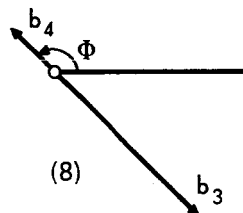(6)
$a_1 = 2, a_2 = 1, \theta = 0°$
$\psi_1 = -60°$
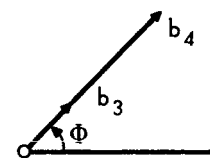
(7)
$a_1 = 2, a_2 = 1, \theta = 0$
$\psi_1 = -90°$

(8)
$a_1 = 2, a_2 = 1, \theta = 180°$
$\psi_1 = -90°$

(9)
$a_1 = 2, a_2 = 1, \theta = 180°$
$\psi_1 = +90°$

CONSERVATION OF ENERGY CONDITION: $a_1^2 + a_2^2 = b_3^2 + b_4^2$

$\Phi = (\pi - \psi_1)/2 = $ PHASE SHIFT OF Σ_m DUE TO WEIGHTING CIRCUIT

Figure 5—Phase and Amplitude Relationships in a Weighting Circuit
Pulse I (1–17), Pulse II (8–9)

11

The first seven phasor diagrams depict the situation for a single-plane amplitude-sensing monopulse system (or one channel of a dual-plane system) when a plane wave-front illuminates the antenna from a point in space such that a single pulse of radiated energy is responsible for a sum intensity $a_1 = 2$ and a difference intensity $a_2 = 1$. The parameter ψ_1 can take on all values over its range; only seven are shown. The modified difference channel $\triangle m$ now provides feedback information to minimize b_3. Assuming that ψ_1 can be varied rapidly, so that the target position is sensibly unchanged in the time interval during which the error channel null is attained, the value of ψ_1 (including its sign) becomes the measure of target position when $b_3 = 0$.

The eighth and ninth phasor diagrams illustrate the output relationships when the received plane wavefront arrives from a direction such that $a_1 = 2$, but $a_2 = -1$. These diagrams, together with the preceding seven, illustrate the nature of the π radian ambiguity associated with the phase angle of the error channel previously. Figure 5 shows that:

1. Cophased input signals may result in cophased or antiphased output signals,

2. Antiphased input signals may result in cophased or antiphased output signals.

Equivalently, given $b_3 = 0$ for some ψ_1 ($-\pi/2 \le \psi_1 \le \pi/2$), there exist modified error signals ($\triangle m$) of opposite sign on either side of the displaced boresight indication for unmodified error signals ($\triangle$) of either sign.

It is noted that an ideal or lossless weighting circuit necessarily yields a maximum modified sum intensity $\Sigma_m = b_4$ in terms of the total energy due to a_1 and a_2 for a particular spatial coordinate θ_1 of the target when ψ_1 is of such a value that $b_3 = 0$. In the event that the target moves to some other point θ_2 on the hypothetical unit sphere, the density of the incoming plane wave remaining constant, the intercepts on the secondary patterns change, and the system energy takes on another value in general. As a consequence of this, ψ_1 remaining constant, the maximum sum intensity will not always lie opposite the null indication. The phenomena described will be referred to as a separation of the difference pattern null and the sum pattern maximum is spatial coordinates (θ, φ). The effect is seen in the pattern plots of Figure 3, and the study of this effect for the dual-plane case is one of the objectives of the present analysis. In addition, the relative energy levels of all channels will be determined to provide a direct comparison with the performance of an unscanned system.
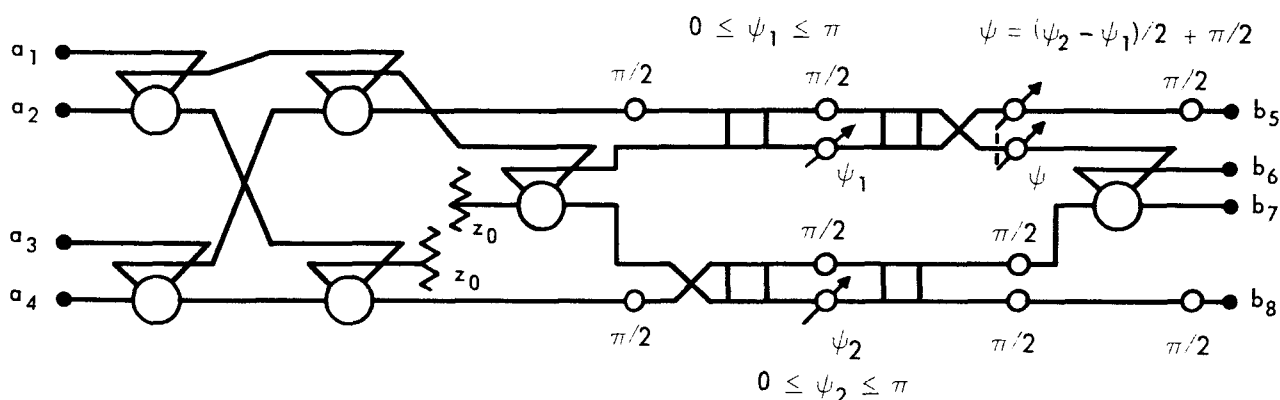
DUAL-PLANE ELECTRONIC BORESIGHT SCANNING CIRCUIT

This report is concerned primarily with the analysis of one circuit and represents an attempt at extending the single-plane amplitude-sensing EBS circuit described by Rhodes in Ref. [2] to a dual-plane EBS circuit, Figure 6. The
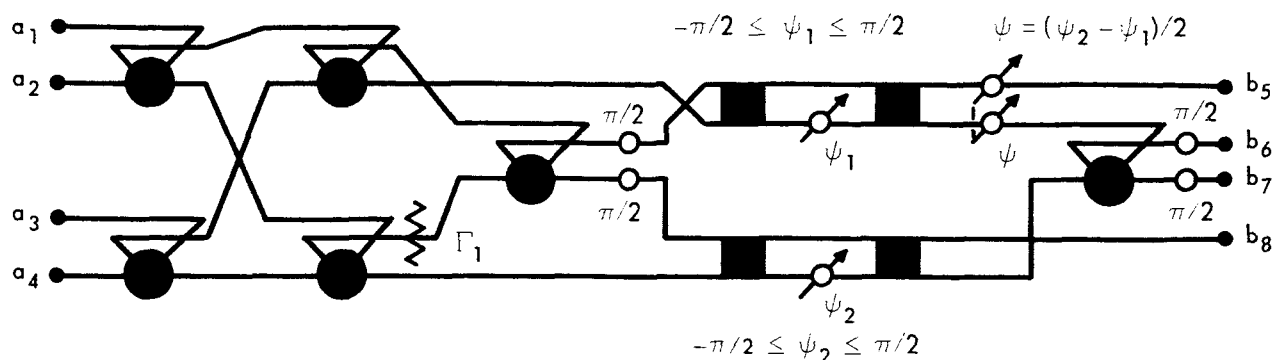
(a) MATHEMATICAL MODEL

(b) PHYSICAL MODEL

Figure 6—Electronic Boresight Scanning Circuit For Dual-Plane
Amplitude-Sensing Monopulse Antenna

mathematical formalism described herein was developed for the purpose of investigating alternative forms of EBS and provides a specific description of the function of every component in the circuit. It is possible to proceed first in a purely intuitive manner, however, by taking into account the basic properties of ring and square hybrids and, particularly, the properties of combinations of junctions such as the weighting circuit. For the case of two error signals, two weighting circuits appear to be a logical choice for displacing the bore sight null in each of two orthogonal planes in space. Splitting of the sum signal follows to obtain two weighting circuits which are roughly analogous to the single-plane circuit. The remainder of the dual-plane circuit is associated with phase normalization to compensate for (1) the phase changes introduced by the hybrid junction which splits the sum signal, and (2) the continuously variable phase changes introduced by the weighting circuits themselves, and finally (3) the phase change incurred at the combining hybrid. The latter should produce a coherent sum channel similar to that of an unscanned system.

Junctions which exhibit the basic properties of ring hybrids and square hybrids can then be arranged with suitable phase shifters and fixed delay lines as shown in Figure 6. The circuit of Figure 6(a) may be regarded as a mathematical model which ignores such issues as the minimum number of line crossovers, minimum line length, and physically realizable phase delays $\psi_i \geq 0$. It is noted that the unscanned or rest condition of this EBS circuit is given by $\psi_{1_r} = \psi_{2_r} = 0$, and $-\pi/2 \leq \psi_1 \leq \pi/2$, $-\pi/2 \leq \psi_2 \leq \pi/2$ is allowed at present in the mathematical model. A suitable physical version is presented as Figure 6(b), but is not utilized in the analysis.

SCATTERING- AND TRANSFER-MATRIX NOTATION

It is convenient, although not essential, to treat circuit problems such as that of Figure 6 in terms of the scattering-matrix analysis of ferrite devices. The notation of Lax and Button of the Lincoln Laboratories, ref. [6], pp. 506-539, will be used for most of this report with certain exceptions evidenced in the detailed development to follow. Additional background on scattering matrix notation can be found in ref. [7], pp. 401-479; ref. [8], pp. 516-530; ref. [9], pp. 350-375 and ref. [10], Chapter IV. Some discretion is required in making comparisons between the references cited above and others found in the literature as there appears to be no preferred or accepted set of conventions, which sometimes leads to confusion. Since the scattering matrix does not lend itself to multiplication it is desirable to convert it to a transfer matrix that admits non-commutative multiplication with other transfer matrices. The conventions adopted in this report will be made definite by means of a detailed conversion from the scattering matrix to the transfer matrix for a junction having the form of a ring-type coaxial hybrid. (See Appendix). All other transfer matrixes used herein are derivable in exactly the same manner and are also tabulated in the Appendix together with their associated scattering matrices.

The individual junctions such as ring hybrids, square hybrids, etc. can be described completely in terms of transformations in a 4-dimensional linear vector space, ref. [8], in which the terminal quantities (i.e. input and output at each port) may be considered as basis vectors. A scattering matrix transformation relates the output at a given port to the inputs at all ports and its elements are complex reflection and transmission coefficients for a chain of junctions. A transfer matrix transformation relates an output or an input on the "right" of a chain of junctions to the inputs and outputs on the "left" of that chain. Elements of the transfer matrix are complex transmission coefficients only. A chain consisting of one junction is admissible for either the scattering or transfer matrices. The respective transformations are given by $\overline{b} = S\overline{a}$ and $\overline{g} = T\overline{h}$. It is necessary to consider the transformation as being defined over the field (F) of complex values (C). Since the circuit of Figure 6 contains pairs of hybrids, the immediate problem of analyzing that circuit lies in an 8-dimensional vector

space $V_n(F) = V_8(C)$. It turns out that eight basis vectors can be made sufficient to span the vector space for this problem even though the dissipative or quadrapolar load termination of the conventional comparator circuit indicates a non-zero kernel, ref. [8], p. 142-146, or a variation in the number of ports at this interface. Ordinarily other means are required to succeed in problems of this type, and may involve rectangular matrices, ref. [9], p. 1. In this instance, the problem is relatively simple and, since only one transformation corresponding to a physical termination occurs <u>within</u> the chain of fifteen transformations, the difficulty is avoided by regarding the transmission coefficient Γ of that load as a quantity arbitrarily close to zero. The inverse of Γ is then well-defined and square matrices are retained for the entire problem. It will be shown that the above restriction on Γ can finally be removed for both the transmitting and receiving cases.

TRANSFORMATIONS OF THE CHAIN MATRIX IN $V_8(C)$

Referring once again to Figure 6, the associative property of matrix multiplication is now used to separate the problem into several parts for convenience in displaying the product of 15 transformations of the input signals (a_1, a_2, a_3, a_4) provided by the antenna. It is noted that the operation of matrix multiplication is not, in general, commutative and requires that the order $T_{eq.} = T_n T_{n-1} \cdots T_1$ $= T_{15} T_{14} \cdots T_1$ be preserved under the conventions previously adopted (Appendix) for the transfer matrices. From a consideration of the fundamental properties of the weighting circuit and the other components, the circuit arrangement given in Figure 6 should provide two orthogonal error channels similar to those described for the single-plane case in Rhodes. The <u>sum</u> input to each weighting package is reduced by a factor of $1/\sqrt{2}$ in voltage, however, and the combined phase correction $\psi = (\psi_2 - \psi_1)/2$ should make possible a continuous coherent recombination of the modified sum signals emanating from the weighting packages. The values ψ_1 and ψ_2 should be capable of restoring the null condition for both modified error channels simultaneously. That is, $\Delta_{EL} = \Delta_{AZ} = 0$ is sought and the modified sum channel signal should be maximized. The chain multiplication $T_{eq.} = T_{15} T_{14} \cdots T_1$ is carried out for completeness and to verify the overall result.

The conventional sum and difference monopulse network is readily described by a transformation $_\bullet T_2 \,_\sigma T_1 \,_\bullet T_1$, where an assumed form only is taken for the ring hybrid elements as indicated in the Appendix. Actual physical forms vary in practice, usually by some phase shift associated with the reference planes or by a crossover of the input or output cables. More involved variations can be identified, especially when waveguide is employed, but these will not be considered here since the specific description of a particular junction can always be accommodated. It is sufficient to utilize the form $_\bullet T_{ij}$ of the Appendix for the ring hybrid.

Then

$$_\bullet T_2 \; _\sigma T_1 \; _\bullet T_1 \; =$$

$$\left(\frac{j}{\sqrt{2}}\right)^2
\begin{bmatrix}
1 & 0 & 1 & 0 & & & & \\
0 & -1 & 0 & -1 & & & & \\
1 & 0 & -1 & 0 & & 0 & & \\
0 & -1 & 0 & 1 & & & & \\
& & & & 1 & 0 & 1 & 0 \\
& & & & 0 & -1 & 0 & -1 \\
& 0 & & & 1 & 0 & -1 & 0 \\
& & & & 0 & -1 & 0 & 1
\end{bmatrix}
\begin{bmatrix}
1 & & & & & & & \\
& 1 & & & & & & \\
& & 0 & -1 & & & & \\
& & & 0 & -1 & & & \\
& & 1 & & 0 & & & \\
& & 1 & & & 0 & & \\
& & & & & & 1 & \\
& & & & & & & 1
\end{bmatrix}
\begin{bmatrix}
1 & 0 & 1 & 0 & & & & \\
0 & -1 & 0 & -1 & & & & \\
1 & 0 & -1 & 0 & & 0 & & \\
0 & -1 & 0 & 1 & & & & \\
& & & & 1 & 0 & 1 & 0 \\
& & & & 0 & -1 & 0 & -1 \\
& 0 & & & 1 & 0 & -1 & 0 \\
& & & & 0 & -1 & 0 & 1
\end{bmatrix} \; =$$

$$-\frac{1}{2}
\begin{bmatrix}
1 & 0 & 1 & 0 & 1 & 0 & 1 & 0 \\
0 & 1 & 0 & 1 & 0 & 1 & 0 & 1 \\
1 & 0 & 1 & 0 & -1 & 0 & -1 & 0 \\
0 & 1 & 0 & 1 & 0 & -1 & 0 & -1 \\
1 & 0 & -1 & 0 & 1 & 0 & -1 & 0 \\
0 & 1 & 0 & -1 & 0 & 1 & 0 & -1 \\
1 & 0 & -1 & 0 & -1 & 0 & 1 & 0 \\
0 & 1 & 0 & -1 & 0 & -1 & 0 & 1
\end{bmatrix}$$

where $_\sigma T_1$ is an elementary matrix of the second kind, ref. [8], p. 193. By using the relation $\overline{g} = T\overline{h}$ for the result above it is easily verified that

$$-2b_5 = a_1 + a_2 + a_3 + a_4, \qquad (\Sigma, \; \text{Sum channel})$$

$$-2b_6 = (a_1 + a_2) - (a_3 + a_4), \qquad (\Delta_1, \; \text{error channel})$$

16

$$-2b_7 = (a_1 + a_3) - (a_2 + a_4), \quad (Q, \text{ quadrupolar load})$$

$$-2b_8 = (a_1 + a_4) - (a_2 + a_3), \quad (\Delta_2, \text{ error channel})$$

The equation $\bar{g} = T\bar{h}$ also yields four similar output equations associated with the transmitting case, but these are not written explicitly since the present EBS problem pertains only to receiving phenomena.

Next, the matrix representatives of the quadrupolar load termination ($_\Gamma T_1$), the cable crossover ($_\sigma T_2$), the sum-channel power divider ($_\bullet T_3$), and the phase normalization lines ($_\beta T_1$) are annexed to the product by forming ($_\beta T_1 \; _\bullet T_3 \; _\sigma T_2 \; _\Gamma T_1$) which is given by:

where $_\beta T_1$ and $_\Gamma T_1$ are elementary matrices of the first kind. Most of the matrix products above are of an extremely simple nature and lead directly to the result

$$(_\beta T_1 \; _\bullet T_3 \; _\sigma T_2 \; _\Gamma T_1) \; (_\bullet T_2 \; _\sigma T_1 \; _\bullet T_1) = (_\beta T_1 \; _\bullet T_3 \; _\sigma T_2 \; _\Gamma T_1 \; _\bullet T_2 \; _\sigma T_1 \; _\bullet T_1) \cdot$$

From this product, given in matrix form as

$$
-\frac{1}{2}
\left[
\begin{array}{cccc|cccc}
1 & 0 & 1 & 0 & -1 & 0 & -1 & 0 \\[2mm]
0 & 1 & 0 & 1 & 0 & -1 & 0 & -1 \\[2mm]
\tfrac{1}{\sqrt{2}}(1+\Gamma_1) & 0 & \tfrac{1}{\sqrt{2}}(1-\Gamma_1) & 0 & \tfrac{1}{\sqrt{2}}(1+\Gamma_1) & 0 & \tfrac{1}{\sqrt{2}}(1-\Gamma_1) & 0 \\[2mm]
0 & \tfrac{1}{\sqrt{2}}(1+\Gamma_1^{-1}) & 0 & \tfrac{1}{\sqrt{2}}(1-\Gamma_1^{-1}) & 0 & \tfrac{1}{\sqrt{2}}(1+\Gamma_1^{-1}) & 0 & \tfrac{1}{\sqrt{2}}(1-\Gamma_1^{-1}) \\[2mm]
\tfrac{1}{\sqrt{2}}(1-\Gamma_1) & 0 & \tfrac{1}{\sqrt{2}}(1+\Gamma_1) & 0 & \tfrac{1}{\sqrt{2}}(1-\Gamma_1) & 0 & \tfrac{1}{\sqrt{2}}(1+\Gamma_1) & 0 \\[2mm]
0 & \tfrac{1}{\sqrt{2}}(1-\Gamma_1^{-1}) & 0 & \tfrac{1}{\sqrt{2}}(1+\Gamma_1^{-1}) & 0 & \tfrac{1}{\sqrt{2}}(1-\Gamma_1^{-1}) & 0 & \tfrac{1}{\sqrt{2}}(1+\Gamma_1^{-1}) \\[2mm]
1 & 0 & -1 & 0 & -1 & 0 & 1 & 0 \\[2mm]
0 & 1 & 0 & -1 & 0 & -1 & 0 & 1
\end{array}
\right]
$$

it is easily shown, via $\bar{g} = T\bar{h}$, that the original received signals have been transformed so that

$$-2\,b_5 = (a_1 + a_2) - (a_3 + a_4), \qquad\qquad (\Delta_1)$$

$$-2\,b_6 = \frac{1}{\sqrt{2}}\,(a_1 + a_2 + a_3 + a_4) \quad \text{when } \Gamma_1 = 0, \quad (\Sigma/\sqrt{2})$$

$$-2\,b_7 = \frac{1}{\sqrt{2}}\,(a_1 + a_2 + a_3 + a_4) \quad \text{when } \Gamma_1 = 0, \quad (\Sigma/\sqrt{2})$$

$$-2\,b_8 = (a_1 + a_4) - (a_2 + a_3), \qquad\qquad (\Delta_2).$$

It is seen that the four channels are either in phase or at most anti-phase which is consistent with (1) the fundamental assumption that the signals $(a_1,\ a_2,\ a_3,\ a_4)$ derived from the antenna are ideally co-phased in a pure amplitude sensing

18

system and (2) the monopulse postulate that the sensing ratio for a positive angle of arrival is the inverse of the ratio for an equal negative angle, ref. [2], pp. 20-26. (Multiplicative and additive sensing ratios, $r_m(u) = P(u)/P(-u)$ and $r_a(u) = P_0(u)/P_e(u)$ have been defined. $P(u)$ and $P(-u)$ are related to secondary beam intensities. $P_0(u)$ and $P_e(u)$ are odd and even functions derived from the former.) Subsequent development of the EBS network will lead to a violation of the postulate given above due to a lack of symmetry about the boresight. The first postulate, which states that monopulse angle information appears in the form of a ratio, will be preserved.

In order to obtain two weighting circuits which are identical in all respects, except for the parameters ψ_1, ψ_2 related to boresight displacement in two orthogonal directions, the outputs thus far obtained will be permuted by means of matrix $_\sigma T_3$ below.

$$
\begin{bmatrix}
0 - - - 1 & & & & \\
& 0 - | - - 1 & & & \\
& & & & \\
1 - | - 0 & & & \\
& 1 - - - 0 & & & \\
\hline
& & 1 & & \\
& & & 1 & \\
& & & & 1 \\
& & & & & 1 \\
& & & & & & 1
\end{bmatrix}
$$

Matrix ($_\sigma T_3$ $_\beta T_1$ $_\bullet T_3$ $_\sigma T_2$ $_\Gamma T_1$ $_\bullet T_2$ $_\sigma T_1$ $_\bullet T$) is the same as the preceding result with the indicated row permutation 1 $\leftrightarrow$ 3, 2 $\leftrightarrow$ 4 and is therefore not written out here. The result obtained after operating with $_\sigma T_3$ will appear in the final result as one of two factors which completely describe the EBS circuit of Figure 6. The second factor is determined as follows.

Forming the transfer matrix for both weighting packages, $_\bullet T_1$ $_\beta T_2$ $_\bullet T_2$,

$$\left(\frac{1}{\sqrt{2}}\right)
\begin{bmatrix}
\begin{array}{cc|cc}
1 & 0 & j & 0 \\
0 & 1 & 0 & -j \\
\hline
j & 0 & 1 & 0 \\
0 & -j & 0 & 1
\end{array} & \text{\Large 0} \\[6pt]
\text{\Large 0} &
\begin{array}{cc|cc}
1 & 0 & j & 0 \\
0 & 1 & 0 & -j \\
\hline
j & 0 & 1 & 0 \\
0 & -j & 0 & 1
\end{array}
\end{bmatrix}
\;(1)\;
\begin{bmatrix}
1 & & & & & & & \\
& 1 & & & & & & \\
& & e^{-j\psi_1} & & & & & \\
& & & e^{j\psi_1} & & & & \\
& & & & 1 & & & \\
& & & & & 1 & & \\
& & & & & & e^{-j\psi_2} & \\
& & & & & & & e^{j\psi_2}
\end{bmatrix}
\left(\frac{1}{\sqrt{2}}\right)
\begin{bmatrix}
\begin{array}{cc|cc}
1 & 0 & j & 0 \\
0 & 1 & 0 & -j \\
\hline
j & 0 & 1 & 0 \\
0 & -j & 0 & 1
\end{array} & \text{\Large 0} \\[6pt]
\text{\Large 0} &
\begin{array}{cc|cc}
1 & 0 & j & 0 \\
0 & 1 & 0 & -j \\
\hline
j & 0 & 1 & 0 \\
0 & -j & 0 & 1
\end{array}
\end{bmatrix} =$$

$$\frac{1}{2}
\begin{bmatrix}
\begin{array}{cccc}
(1-e^{-j\psi_1}) & 0 & j(1+e^{-j\psi_1}) & 0 \\
0 & (1-e^{j\psi_1}) & 0 & -j(1+e^{j\psi_1}) \\
j(1+e^{-j\psi_1}) & 0 & (-1+e^{-j\psi_1}) & 0 \\
0 & -j(1+e^{j\psi_1}) & 0 & (-1+e^{j\psi_1})
\end{array} & \text{\Large 0} \\[10pt]
\text{\Large 0} &
\begin{array}{cccc}
(1-e^{-j\psi_2}) & 0 & j(1+e^{-j\psi_2}) & 0 \\
0 & (1-e^{j\psi_2}) & 0 & -j(1+e^{j\psi_2}) \\
j(1+e^{-j\psi_2}) & 0 & (-1+e^{-j\psi_2}) & 0 \\
0 & -j(1+e^{j\psi_2}) & 0 & (-1+e^{j\psi_2})
\end{array}
\end{bmatrix}$$

For simplicity in subsequent operations let

$$z_1 = 1 - e^{-j\psi_1} \qquad z_5 = 1 - e^{j\psi_1}$$

$$z_2 = 1 + e^{-j\psi_1} \qquad z_6 = 1 + e^{j\psi_1}$$

$$z_3 = 1 - e^{-j\psi_2} \qquad z_7 = 1 - e^{j\psi_2}$$

$$z_4 = 1 + e^{-j\psi_2} \qquad z_8 = 1 + e^{j\psi_2}$$

Then the factor ($_\beta T_4 \ _\bullet T_4 \ _\sigma T_4 \ _\beta T_3 \ _\blacksquare T_2 \ _\beta T_2 \ _\blacksquare T_1$) is formed using the following matrices:

$$_\sigma T_3 = \begin{bmatrix} e^{-j\psi} & & & & & & & \\ & e^{j\psi} & & & & & & \\ & & e^{-j\psi} & & & & & \\ & & & e^{j\psi} & & & & \\ & & & & 1 & & & \\ & & & & & 1 & & \\ & & & & & & 1 & \\ & & & & & & & 1 \end{bmatrix} \quad ; \quad _\sigma T_4 = \begin{bmatrix} 1 & & & & & & & \\ & 1 & & & & & & \\ & & 1 & & & & & \\ & & & 1 & & & & \\ & & & & 0 & & & -1 \\ & & & & & 0 & & -1 \\ & & & & & & 1 & 0 \\ & & & & 1 & & & 0 \end{bmatrix}$$

where $\psi = (\psi_2 - \psi_1)/2$

$$_\bullet T_4 = \begin{bmatrix} 1 & & & & & & & \\ & 1 & & & & & & \\ & & \dfrac{j}{\sqrt{2}} & 0 & \dfrac{j}{\sqrt{2}} & 0 & & \\ & & 0 & -\dfrac{j}{\sqrt{2}} & 0 & -\dfrac{j}{\sqrt{2}} & & \\ & & \dfrac{j}{\sqrt{2}} & 0 & -\dfrac{j}{\sqrt{2}} & 0 & & \\ & & 0 & -\dfrac{j}{\sqrt{2}} & 0 & \dfrac{j}{\sqrt{2}} & & \\ & & & & & & 1 & \\ & & & & & & & 1 \end{bmatrix} \quad ; \quad _\beta T_4 = \begin{bmatrix} 1 & & & & & & & \\ & 1 & & & & & & \\ & & -j & & & & & \\ & & & +j & & & & \\ & & & & -j & & & \\ & & & & & +j & & \\ & & & & & & 1 & \\ & & & & & & & 1 \end{bmatrix}$$

Upon completion of the indicated operations, the two factors which describe the entire EBS circuit enter into a product, $(\,_\beta T_4 \;\; _\bullet T_4 \;\; _\sigma T_4 \;\; _\beta T_3 \;\; _\blacksquare T_2 \;\; _\beta T_2 \;\; _\blacksquare T_1 \,)$ $(\,_\sigma T_3 \;\; _\beta T_1 \;\; _\bullet T_3 \;\; _\sigma T_2 \;\; _\Gamma T_1 \;\; _\bullet T_2 \;\; _\sigma T_1 \;\; _\bullet T_1)$, and yield the final result $T_{eq.}$ given below.

$$\frac{1}{2} \begin{bmatrix} z_1 e^{-j\psi} & 0 & jz_2 e^{-j\psi} & 0 & 0 & 0 & 0 & 0 \\ 0 & z_5 e^{j\psi} & 0 & -jz_6 e^{j\psi} & 0 & 0 & 0 & 0 \\ j\dfrac{z_2}{\sqrt{2}}e^{-j\psi} & 0 & -\dfrac{z_1}{\sqrt{2}}e^{-j\psi} & 0 & j\dfrac{z_4}{\sqrt{2}} & 0 & -\dfrac{z_3}{\sqrt{2}} & 0 \\ 0 & -j\dfrac{z_6}{\sqrt{2}}e^{j\psi} & 0 & -\dfrac{z_5}{\sqrt{2}}e^{j\psi} & 0 & -j\dfrac{z_8}{\sqrt{2}} & 0 & -\dfrac{z_7}{\sqrt{2}} \\ j\dfrac{z_2}{\sqrt{2}}e^{-j\psi} & 0 & -\dfrac{z_1}{\sqrt{2}}e^{-j\psi} & 0 & -j\dfrac{z_4}{\sqrt{2}} & 0 & \dfrac{z_3}{\sqrt{2}} & 0 \\ 0 & -j\dfrac{z_6}{\sqrt{2}}e^{j\psi} & 0 & -\dfrac{z_5}{\sqrt{2}}e^{j\psi} & 0 & j\dfrac{z_8}{\sqrt{2}} & 0 & \dfrac{z_7}{\sqrt{2}} \\ 0 & 0 & 0 & 0 & z_3 & 0 & jz_4 & 0 \\ 0 & 0 & 0 & 0 & 0 & z_7 & 0 & -jz_8 \end{bmatrix}$$

22

$$\frac{1}{2}\begin{bmatrix}
\frac{1}{\sqrt{2}}(1+\Gamma_1) & 0 & \frac{1}{\sqrt{2}}(1-\Gamma_1) & 0 & \frac{1}{\sqrt{2}}(1+\Gamma_1) & 0 & \frac{1}{\sqrt{2}}(1-\Gamma_1) & 0 \\
0 & \frac{1}{\sqrt{2}}(1+\Gamma_1^{-1}) & 0 & \frac{1}{\sqrt{2}}(1-\Gamma_1^{-1}) & 0 & \frac{1}{\sqrt{2}}(1+\Gamma_1^{-1}) & 0 & \frac{1}{\sqrt{2}}(1-\Gamma_1^{-1}) \\
1 & 0 & 1 & 0 & -1 & 0 & -1 & 0 \\
0 & 1 & 0 & 1 & 0 & -1 & 0 & -1 \\
\frac{1}{\sqrt{2}}(1-\Gamma_1) & 0 & \frac{1}{\sqrt{2}}(1+\Gamma_1) & 0 & \frac{1}{\sqrt{2}}(1-\Gamma_1) & 0 & \frac{1}{\sqrt{2}}(1+\Gamma_1) & 0 \\
0 & \frac{1}{\sqrt{2}}(1-\Gamma_1^{-1}) & 0 & \frac{1}{\sqrt{2}}(1+\Gamma_1^{-1}) & 0 & \frac{1}{\sqrt{2}}(1-\Gamma_1^{-1}) & 0 & \frac{1}{\sqrt{2}}(1+\Gamma_1^{-1}) \\
1 & 0 & -1 & 0 & -1 & 0 & 1 & 0 \\
0 & 1 & 0 & -1 & 0 & -1 & 0 & 1
\end{bmatrix}$$

$$\bar{g} = T_{eq}\,\bar{h},$$

$$-4\begin{bmatrix} b_5 \\ a_5 \\ b_6 \\ a_6 \\ b_7 \\ a_7 \\ b_8 \\ a_8 \end{bmatrix} = \begin{bmatrix}
T_{11} & 0 & T_{13} & 0 & T_{15} & 0 & T_{17} & 0 \\
0 & T_{22} & 0 & T_{24} & 0 & T_{26} & 0 & T_{28} \\
T_{31} & 0 & T_{33} & 0 & T_{35} & 0 & T_{37} & 0 \\
0 & T_{42} & 0 & T_{44} & 0 & T_{46} & 0 & T_{48} \\
T_{51} & 0 & T_{53} & 0 & T_{55} & 0 & T_{57} & 0 \\
0 & T_{62} & 0 & T_{64} & 0 & T_{66} & 0 & T_{68} \\
T_{71} & 0 & T_{73} & 0 & T_{75} & 0 & T_{77} & 0 \\
0 & T_{82} & 0 & T_{84} & 0 & T_{86} & 0 & T_{88}
\end{bmatrix}\begin{bmatrix} a_1 \\ b_1 \\ a_2 \\ b_2 \\ a_3 \\ b_3 \\ a_4 \\ b_4 \end{bmatrix}$$

23

DIRECT SUMS AND REDUCTION OF RESULTS

Prior to writing out the functional relationships for the elements of T_{eq}, a rearrangement of the input and output terms of the column vectors (matrices) leads to a simplification.

$$-4 \begin{bmatrix} b_5 \\ b_6 \\ b_7 \\ b_8 \\ a_5 \\ a_6 \\ a_7 \\ a_8 \end{bmatrix} = \left[\begin{array}{cccc|cccc} T_{11} & T_{13} & T_{15} & T_{17} & & & & \\ T_{31} & T_{33} & T_{35} & T_{37} & & & & \\ T_{51} & T_{53} & T_{55} & T_{57} & & & 0 & \\ T_{71} & T_{73} & T_{75} & T_{77} & & & & \\ \hline & & & & T_{22} & T_{24} & T_{26} & T_{28} \\ & & 0 & & T_{42} & T_{44} & T_{46} & T_{48} \\ & & & & T_{62} & T_{64} & T_{66} & T_{68} \\ & & & & T_{82} & T_{84} & T_{86} & T_{88} \end{array} \right] \begin{bmatrix} a_1 \\ a_2 \\ a_3 \\ a_4 \\ b_1 \\ b_2 \\ b_3 \\ b_4 \end{bmatrix}$$

Now $\bar{g}' = T'_{eq.} \, \bar{h}'$ and

$$T'_{eq.} = \left[\begin{array}{c|c} T_1 & \\ \hline & T_2 \end{array} \right] = T_1 \oplus T_2, \text{ a } \underline{direct} \text{ sum of matrices,}$$
ref. [11] p. 25, ref. [12] pp. 165-169.

The decomposition of $T'_{eq.}$ into a direct sum and the accompanying decomposition of $V_8(C)$ into two invariant subspaces clearly distinguishes between the transmitting and receiving modes of operation. Since only the latter is of interest here the elements of T_1 only will be given. It is possible to set Γ_1 equal to zero in subsequent expressions since the inverse of Γ_1 (or Γ_1^{-1}) does not appear in any of the relationships. Then the final output signals are given by:

$$-4 b_5 = a_1 T_{11} + a_2 T_{13} + a_3 T_{15} + a_4 T_{17}, \quad (\Delta_1)$$

$$-4 b_6 = a_1 T_{31} + a_2 T_{33} + a_3 T_{35} + a_4 T_{37}, \quad (\Sigma)$$

$$-4\,b_7 = a_1\,T_{51} + a_2\,T_{53} + a_3\,T_{55} + a_4\,T_{57}, \quad \text{(Load)}$$

$$-4\,b_8 = a_1\,T_{71} + a_2\,T_{73} + a_3\,T_{75} + a_4\,T_{77}, \quad (\Delta_2)$$

where

$$T_{11} = T_{13} = \left(\frac{Z_1}{\sqrt{2}} + j\,Z_2\right)\,e^{-j\psi}$$

$$T_{15} = T_{17} = \left(\frac{Z_1}{\sqrt{2}} - j\,Z_2\right)\,e^{-j\psi}$$

$$T_{31} = \left(j\,\frac{Z_2}{2} - \frac{Z_1}{\sqrt{2}}\right)\,e^{-j\psi} + j\,\frac{Z_4}{2} - \frac{Z_3}{\sqrt{2}}$$

$$T_{33} = \left(j\,\frac{Z_2}{2} - \frac{Z_1}{\sqrt{2}}\right)\,e^{-j\psi} + j\,\frac{Z_4}{2} + \frac{Z_3}{\sqrt{2}}$$

$$T_{35} = \left(j\,\frac{Z_2}{2} + \frac{Z_1}{\sqrt{2}}\right)\,e^{-j\psi} + j\,\frac{Z_4}{2} + \frac{Z_3}{\sqrt{2}}$$

$$T_{37} = \left(j\,\frac{Z_2}{2} + \frac{Z_1}{\sqrt{2}}\right)\,e^{-j\psi} + j\,\frac{Z_4}{2} - \frac{Z_3}{\sqrt{2}}$$

$$T_{51} = \left(j\,\frac{Z_2}{2} - \frac{Z_1}{\sqrt{2}}\right)\,e^{-j\psi} - j\,\frac{Z_4}{2} + \frac{Z_3}{\sqrt{2}}$$

$$T_{53} = \left(j\,\frac{Z_2}{2} - \frac{Z_1}{\sqrt{2}}\right)\,e^{-j\psi} - j\,\frac{Z_4}{2} - \frac{Z_3}{\sqrt{2}}$$

$$T_{55} = \left(j\,\frac{Z_2}{2} + \frac{Z_1}{\sqrt{2}}\right)\,e^{-j\psi} - j\,\frac{Z_4}{2} - \frac{Z_3}{\sqrt{2}}$$

$$T_{57} = \left(j\,\frac{Z_2}{2} + \frac{Z_1}{\sqrt{2}}\right)\,e^{-j\psi} - j\,\frac{Z_4}{2} + \frac{Z_3}{\sqrt{2}}$$

25

$$T_{71} = T_{77} = \frac{Z_3}{\sqrt{2}} + jZ_4$$

$$T_{73} = T_{75} = \frac{Z_3}{\sqrt{2}} - jZ_4.$$

It is of some interest to examine the final output signals for the case when the EBS circuit is in the rest condition corresponding to $\psi_1 = \psi_2 = 0$. Then $\psi = \psi_2 - \psi_1/2 = 0$ also and, if a plane wave is incident on the aperture from the undisplaced boresight, $a_1 = a_2 = a_3 = a_4$. For a given beam cluster let this intensity equal a_0. It is evident that

$$b_5 = b_7 = b_8 = 0 \qquad (\triangle_1, \text{ load}, \triangle_2),$$

$$-4b_6 = 2j(a_1 + a_2 + a_3 + a_4) = 2j(4a_0) \qquad (\Sigma).$$

From the latter equation, $b_6 = -2ja_0$ and the system energy $\mathcal{E}_\Sigma$ appears at the sum port (6) and equals $|b_6|^2$ or $4a_0^2$. For this special case all of the energy appears at the sum port and is identical to that of a conventional monopulse installation with an ideal circuit. The value $\mathcal{E}_\Sigma = 4a_0^2$ will therefore be used as a reference in comparing the signal strength of the sum or telemetry channel for less restrictive examples ($\psi_1 \neq 0$, $\psi_2 \neq 0$, $\psi_1 \neq \psi_2$, source of radiation displaced from $\theta = 0$) since it represents the energy available when a mechanically scanned antenna is optimally directed toward the source of radiation in a tracking operation.

Although the elements of T_1 now completely describe the operation of the circuit and a computer could be utilized at this point to obtain field plots for arbitrary trajectories over the antenna, it is possible in this particular instance to achieve further simplification of the four expressions for the output quantities

(Σ = sum, $\triangle_2$ = error channel,

$\triangle_1$ = error channel, L = load channel).

It may not be desirable, or even possible, to reduce a given problem to the $T_{eq.} = T_1 \oplus T_2$ form in some instances, in which case the matrix product $T_n T_{n-1} \cdots T_1$ can be solved by machine.

26

The simplification is effected for the receiving case by identifying factors related to the output signals from a conventional dual-plane sum-and-difference network. Using the direct sum decomposition for the receiving case,

$$\overline{g}' = T_1 \overline{h}' = \begin{bmatrix} g_1 \\ g_3 \\ g_5 \\ g_7 \end{bmatrix} = T_1 \begin{bmatrix} h_1 \\ h_3 \\ h_5 \\ h_7 \end{bmatrix} = \begin{bmatrix} b_5 \\ b_6 \\ b_7 \\ b_8 \end{bmatrix} = \begin{bmatrix} T_{11} & T_{13} & | & T_{15} & T_{17} \\ T_{31} & T_{33} & | & T_{35} & T_{37} \\ - & - & - & - & | & - & - & - & - \\ T_{51} & T_{53} & | & T_{55} & T_{57} \\ T_{71} & T_{73} & | & T_{75} & T_{77} \end{bmatrix} \begin{bmatrix} a_1 \\ a_2 \\ a_3 \\ a_4 \end{bmatrix}$$

the following substitutions are made.

$$\frac{\Sigma_c}{\sqrt{2}} = -\frac{1}{2\sqrt{2}} (a_1 + a_2 + a_3 + a_4)$$

$$\Delta_{1c} = -\frac{1}{2} [(a_1 + a_2) - (a_3 + a_4)]$$

$$\Delta_{2c} = -\frac{1}{2} [(a_1 + a_4) - (a_2 + a_3)] .$$

It is noted that the sign of Δ_{1c} and Δ_{2c} depends only on the amplitudes of input signals (a_i) associated with the secondary pattern cluster.

Before proceeding with the simplification, it will be advantageous to review the character of the phase displacements due to a weighting circuit. Under $-\pi/2 \leq \psi_1 \leq \pi/2$ and $|a_1| \geq |a_2|$, it can be seen that the common factors in the expressions for $\tan (\arg b_4)$ always reduce to the quotient $+1/+1$ so that changes in the quadrant of $(\arg b_4)$ are due to the ratio $\cos \psi_1/2 / \sin \psi_1/2$. The numerator is an even function, therefore, the odd function in the denominator is solely responsible for changes in quadrant of Φ. The values $\psi_1 = \pm\pi/2$ determine the bounds on the phase variation of ψ as shown in Fig. 7.
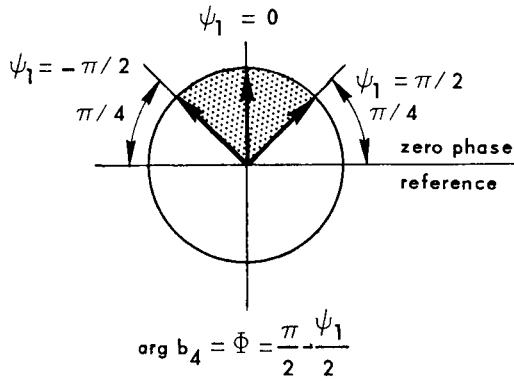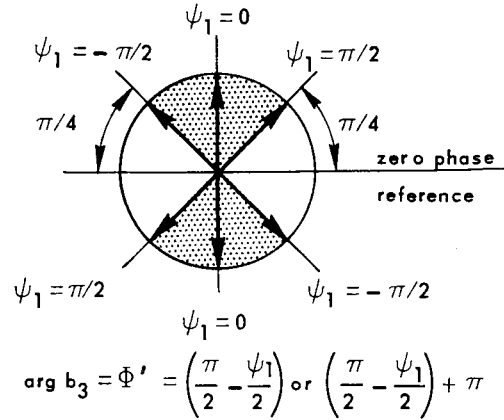
Figure 7—Sum-Channel Phase Diagram

Figure 8—Difference-Channel Phase Diagram

$$\tan (\arg b_4) = \frac{\cos \psi_{1/2} \, (a_1 \cos \psi_{1/2} \pm a_2 \sin \psi_{1/2})}{\sin \psi_{1/2} \, (a_1 \cos \psi_{1/2} \pm a_2 \sin \psi_{1/2})}$$

where $a_1 > 0$, $a_2 \geq 0$ and should not be confused with the set a_i of the input column vector.

The expression for $\tan (\arg b_3)$ is more involved due to the inherent π-radian ambiguity. The ratios of the common factors can now be $+1/+1$ or $-1/-1$. As in the preceding instance, the ratio $\cos \psi_{1/2} \big/ \sin \psi_{1/2}$ can change the quandrant of Φ. If the ratio of common factors is $+1/+1$, then the range of Φ is exactly as before. If the ratio is $-1/-1$, the region in the lower half of the phase diagram, Figure 8, contains the range of angles for the $(\arg b_3)$.

$$\tan (\arg b_3) = \frac{\cos \psi_{1/2} \, (a_1 \sin \psi_{1/2} \pm a_2 \cos \psi_{1/2})}{\sin \psi_{1/2} \, (a_1 \sin \psi_{1/2} \pm a_2 \cos \psi_{1/2})}$$

where $a_1 > 0$, $a_2 \geq 0$.

The generalization to be made is that a_1 and a_2 will be interpreted as $\Sigma_c/\sqrt{2}$ and Δ_{1c}, Δ_{2c} respectively, and $\psi_1\big/2$ may also become $\psi_2\big/2$, as required.

28

Then:

$$\Delta_1 = -\frac{1}{2}\left[\frac{Z_1}{2\sqrt{2}}(a_1 + a_2 + a_3 + a_4) + j\frac{Z_2}{2}(a_1 + a_2 - a_3 - a_4)\right]e^{-j\psi}$$

$$= \left|\frac{\Sigma_c}{\sqrt{2}}\sin\frac{\psi_1}{2} + \Delta_{1c}\cos\frac{\psi_1}{2}\right|e^{j\Phi'_1}e^{-j\psi}$$

where

$$\Phi'_1 = \tan^{-1}\left[\frac{\cos\frac{\psi_1}{2}\left(\frac{\Sigma_c}{\sqrt{2}}\sin\frac{\psi_1}{2} + \Delta_{1c}\cos\frac{\psi_1}{2}\right)}{\sin\frac{\psi_1}{2}\left(\frac{\Sigma_c}{\sqrt{2}}\sin\frac{\psi_1}{2} + \Delta_{1c}\cos\frac{\psi_1}{2}\right)}\right] = \left(\frac{\pi}{2} - \frac{\psi_1}{2}\right) \text{ or } \left(\frac{\pi}{2} - \frac{\psi_1}{2}\right) + \pi$$

and Δ_{1c} is plus or minus, $|\Sigma_c/\sqrt{2}| > |\Delta_{1c}|$

$$\Delta_{2c} = -\frac{1}{2}\left[\frac{Z_3}{2\sqrt{2}}(a_1 + a_2 + a_3 + a_4) + j\frac{Z_4}{2}(a_1 + a_4 - a_2 - a_3)\right]$$

$$= \left|\frac{\Sigma_c}{\sqrt{2}}\sin\frac{\psi_2}{2} + \Delta_{2c}\cos\frac{\psi_2}{2}\right|e^{j\Phi'_2}$$

where

$$\Phi'_2 = \tan^{-1}\left[\frac{\cos\psi_2/2\left(\frac{\Sigma_c}{\sqrt{2}}\sin\psi_2/2 + \Delta_{2c}\cos\psi_2/2\right)}{\sin\psi_2/2\left(\frac{\Sigma_c}{\sqrt{2}}\sin\psi_2/2 + \Delta_{2c}\cos\psi_2/2\right)}\right] = \begin{array}{l}\left(\frac{\pi}{2} - \frac{\psi_2}{2}\right) \text{ or} \\[2mm] \left(\frac{\pi}{2} - \frac{\psi_2}{2}\right) + \pi\end{array}$$

and Δ_{2c} is plus or minus, $|\Sigma_c/\sqrt{2}| > |\Delta_{2c}|$. The a_i (i = 1, 2, 3, 4) here represent the elements of the input column vector and are identical to the E_i (i = 1, 2, 3, 4) in the development of the beam cluster in the Appendix.

29

$$\Sigma = \frac{-1}{4}\left[j\frac{Z_2}{2}(a_1 + a_2 + a_3 + a_4)\,e^{-j\psi} - \frac{Z_1}{\sqrt{2}}(a_1 + a_2 - a_3 - a_4)\,e^{-j\psi} + j\frac{Z_4}{2}(a_1 + a_2 + a_3 + a_4) - \frac{Z_3}{\sqrt{2}}(a_1 + a_4 - a_2 - a_3)\right]$$

$$= \left|\frac{\Sigma_c}{2}\cos\frac{\psi_1}{2} - \frac{\Delta_{1c}}{\sqrt{2}}\sin\frac{\psi_1}{2}\right|e^{j\Phi_1}\,e^{-j\psi} + \left|\frac{\Sigma_c}{2}\cos\frac{\psi_2}{2} - \frac{\Delta_{2c}}{\sqrt{2}}\sin\frac{\psi_2}{2}\right|e^{j\Phi_2}$$

where

$$\Phi_1 = \tan^{-1}\left[\frac{\cos\dfrac{\psi_1}{2}\left(\dfrac{\Sigma_c}{\sqrt{2}}\cos\psi_1/2 - \Delta_{1c}\sin\dfrac{\psi_1}{2}\right)}{\sin\dfrac{\psi_1}{2}\left(\dfrac{\Sigma_c}{\sqrt{2}}\cos\psi_1/2 - \Delta_{1c}\sin\dfrac{\psi_1}{2}\right)}\right] = \left(\frac{\pi}{2} - \frac{\psi_1}{2}\right)$$

$$\Phi_2 = \tan^{-1}\left[\frac{\cos\dfrac{\psi_2}{2}\left(\dfrac{\Sigma_c}{\sqrt{2}}\cos\psi_2/2 - \Delta_{2c}\sin\dfrac{\psi_2}{2}\right)}{\sin\dfrac{\psi_2}{2}\left(\dfrac{\Sigma_c}{\sqrt{2}}\cos\psi_2/2 - \Delta_{2c}\sin\dfrac{\psi_2}{2}\right)}\right] = \left(\frac{\pi}{2} - \frac{\psi_2}{2}\right)$$

and Δ_{2c}, Δ_{1c} are plus or minus, $|\Sigma_c/\sqrt{2}| > |\Delta_{2c}|$ or $|\Delta_{1c}|$

$$L = -\frac{1}{4}\left[j\frac{Z_2}{2}(a_1 + a_2 + a_3 + a_4)\,e^{-j\psi} - \frac{Z_1}{\sqrt{2}}(a_1 + a_2 - a_3 - a_4)\,e^{-j\psi} - j\frac{Z_4}{2}(a_1 + a_2 + a_3 + a_4) + \frac{Z_3}{\sqrt{2}}(a_1 + a_4 - a_2 - a_3)\right]$$

$$= \left|\frac{\Sigma_c}{2}\cos\frac{\psi_1}{2} - \frac{\Delta_{1c}}{\sqrt{2}}\sin\frac{\psi_1}{2}\right|e^{j\Phi_1}\,e^{-j\psi} - \left|\frac{\Sigma_c}{2}\cos\frac{\psi_2}{2} - \frac{\Delta_{2c}}{\sqrt{2}}\sin\frac{\psi_2}{2}\right|e^{j\Phi_2}$$

where Φ_1 and Φ_2 are the same as for the Σ channel.

Since

$$\psi = \frac{\psi_2 - \psi_1}{2},$$

$$\Phi_1 = \frac{\pi}{2} - \frac{\psi_1}{2},$$

$$\Phi_2 = \frac{\pi}{2} - \frac{\psi_2}{2},$$

30

$$\Phi_1' = (\Phi_1) \text{ or } (\Phi_1 + \pi),$$

$$\Phi_2' = (\Phi_2) \text{ or } (\Phi_2 + \pi);$$

the following simplification is achieved.

$$\Delta_1 = \pm \left| \frac{\Sigma_c}{\sqrt{2}} \sin \frac{\psi_1}{2} + \Delta_{1c} \cos \frac{\psi_1}{2} \right| e^{j\Phi_2}$$

$$\Delta_2 = \pm \left| \frac{\Sigma_c}{\sqrt{2}} \sin \frac{\psi_2}{2} + \Delta_{2c} \cos \frac{\psi_2}{2} \right| e^{j\Phi_2}$$

$$L = \pm \left| \left| \frac{\Sigma_c}{2} \cos \frac{\psi_1}{2} - \frac{\Delta_{1c}}{\sqrt{2}} \sin \frac{\psi_1}{2} \right| - \left| \frac{\Sigma_c}{2} \cos \frac{\psi_2}{2} - \frac{\Delta_{2c}}{\sqrt{2}} \sin \frac{\psi_2}{2} \right| \right| e^{j\Phi_2}$$

$$\Sigma = \left[\left| \frac{\Sigma_c}{2} \cos \frac{\psi_1}{2} - \frac{\Delta_{1c}}{\sqrt{2}} \sin \frac{\psi_1}{2} \right| + \left| \frac{\Sigma_c}{2} \cos \frac{\psi_2}{2} - \frac{\Delta_{2c}}{\sqrt{2}} \sin \frac{\psi_2}{2} \right| \right] e^{j\Phi_2}$$

It is noted that two signals are combined in a phase-coherent manner, above, to produce a sum channel (Σ) with unambiguous phase. That is, the Σ becomes a phase reference relative to Δ_1, Δ_2, L channels and may therefore be utilized for product detection or an analogous process. The Δ_2 and Δ_1 channels possess the requisite π-radian ambiguity, as does the L channel, but the latter is of no significance in the present tracking operation.

DISCUSSION OF RESULTS

The results obtained in this report are as follows. An analytical description of a dual-plane amplitude-sensing monopulse EBS system has been obtained via scattering matrix notation and reduced to a simple form. Two satisfactory driving functions have been developed to represent the antenna under simplifying assumptions. The combination of driving functions and chain formulation make possible computer solutions for arbitrary trajectories of a satellite over an EBS-equipped monopulse installation.

The following can now be computed and presented in graphical form.

(1) the exact relationship between the required amounts of electronic phase shift and the null displacement in spatial coordinates

(2) the limits or extent of the null steering capability

(3) all energy relationships among the sum and difference channels in terms of a comparable mechanically scanned system

(4) the quantitative effects of null and sum-maximum separation

(5) the effect on error-slope as a function of the scanning variables ψ_1 and ψ_2.

Preliminary antenna pattern cuts have been obtained via computer and these indicate that the schematic circuit is operating in a satisfactory manner. A second report, now in preparation, will exhibit numerous pattern cuts for the more significant trajectories over the antenna under various operating conditions. Fabrication of coaxial and stripline versions of the EBS circuit have been initiated. A signal simulator has been built to replace the antenna during the preliminary bench-test evaluations. A study of low-loss, high-speed electronic phase-shifters is proceeding concurrently with the work described above. Present plans include an antenna range evaluation of the complete EBS system utilizing a 15-foot parabolic reflector antenna.

APPENDIX I

A brief transfer function analysis of the EBS-servo system is given in this appendix to support the heuristic argument presented in the introduction. In addition, an illustrative simulation of the system was made on an analog computer, and the results are reported here. Since the extent and the manner in which the servo specifications may be relaxed depend upon the outcome of the EBS development, a nominal relaxation, consisting of reductions in servo-loop gain and bandwidth to one half their normal values, was used.

Transfer Function Analysis

In Figure 9(a), the system of Figure 2 is redrawn to present the significant signals and transfer functions. The open-loop transfer function of the EBS loop is KG_1 while G_2 is that of the mechanical servo loop. K relates the pattern-scanning signal and the resulting scanning angle (S). For convenience K is assumed to be frequency independent and of unity magnitude. The effect of bore-sight scanning is indicated by the summation in which the sum of the mechanical motion (M) and the EBS motion (S) produces the boresight (C). Figure 9(a) may be manipulated into either of the forms given in Figures 9(b) and 9(c). The relation between satellite line of sight (R) and the mechanical center line of the dish (M) is shown explicitly in Figure 9(b). If the gain of G_1 is much greater than 1 over the bandwidth of G_2

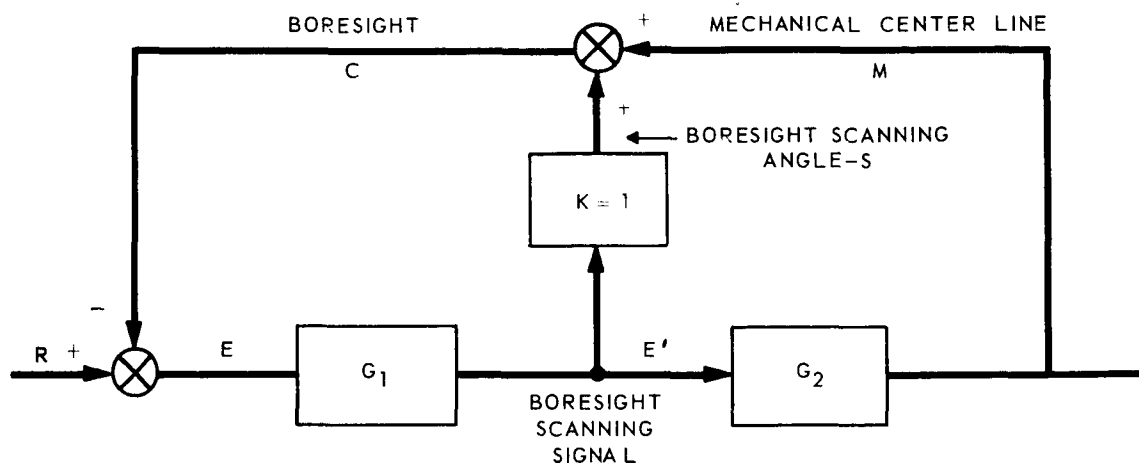$$\frac{G_1}{1 + G_1} \longrightarrow 1$$

and the closed-loop transfer function approaches that of the original system without the EBS loop, that is

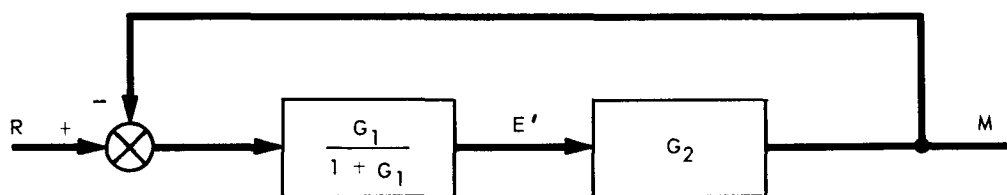$$\frac{M}{R} \approx \frac{G_2}{1 + G_2}$$

demonstrating that the EBS loop has negligible effect upon the mechanical servo loop.

From Figure 9(c) the closed-loop transfer function relating the boresight angle (C) and the satellite line-of-sight angle (R) is
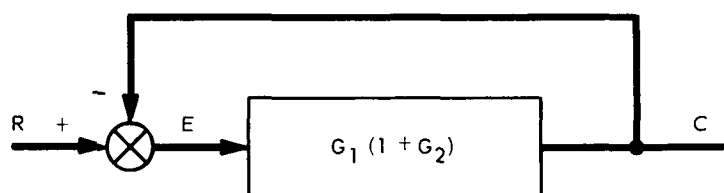
$$\frac{C}{R} = \frac{G_1 (1 + G_2)}{1 + G_1 (1 + G_2)}$$

(a)

(b)

(c)

Figure 9—EBS-Servo Control System Block Diagrams

34

by imposing the additional condition, $|G_2| \ll 1$ at frequencies near the mechanical resonances,

$$\frac{C}{R} \approx \frac{G_1}{1 + G_1}$$

and system performance is essentially independent of the resonant effects. The conditions on G_1 and G_2 are easily met since high-frequency correction components are carried by the EBS loop and the bandwidth of the mechanical servo loop is intentionally restricted.

Simulation Results

The Rosman, North Carolina, 85-foot antenna system was chosen for simulation as the servo loop in the illustrative example. Three system configurations were tested:

1. The present Rosman system

2. The Rosman system with reduced gain and bandwidth

3. The Rosman system with reduced gain and bandwidth and with an EBS loop added.

The closed-loop bandwidths were 1.6 cps for the normal Rosman system, 0.82 cps for the relaxed Rosman system, and 5.0 cps for the EBS loop. The three configurations were tested for step function response, Figure 10; error in following a 0.01 cycle-per-second sine wave, Figure 11; and error due to a step-load disturbance, Figure 12. In each of these figures, the forcing function is recorded at the top, and the responses for the three system configurations are shown in order below.

In Figure 10, the reduced gain and bandwidth are seen to produce an increase in settling time and a reduction in overshoot. Addition of the EBS loop restores the settling time and further reduces the overshoot. In Figure 11, the increased following error, resulting from the system relaxation, is shown while the boresight error in the system with EBS is almost imperceptible. The 0.01 cycle-per-second sine wave approximates the tracking requirements of a 100-mile-high circular orbit. Figure 12 illustrates the reduced response to a load disturbance, such as a wind gust, when the EBS is added. Analysis of additional simulation data demonstrated reductions in hydraulic pressure surges and structural vibration. These effects may be inferred from the more sluggish response to the step input in Figure 10, as well.
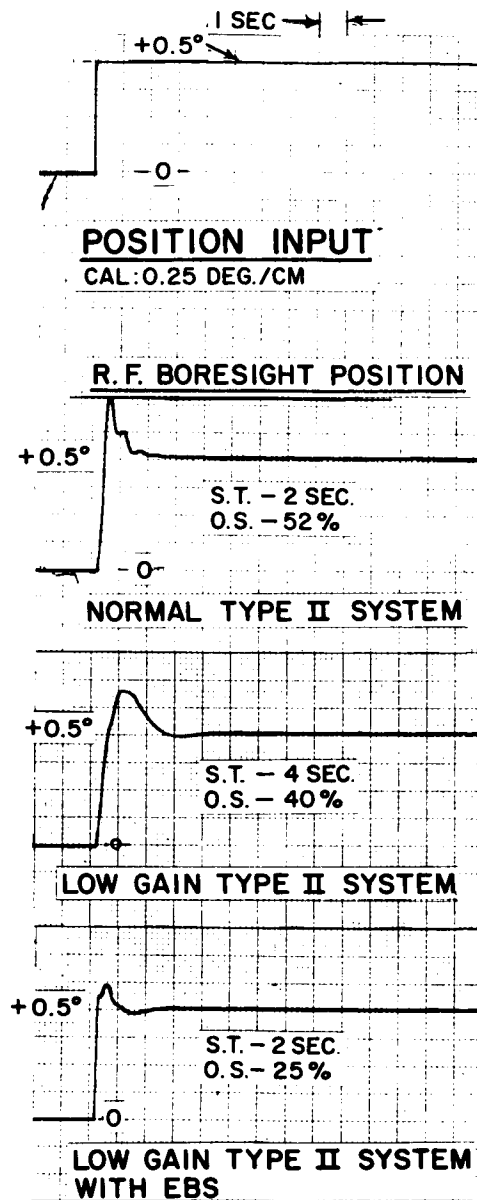
+.1 SEC →| |←

+0.5°

—0—

POSITION INPUT
CAL: 0.25 DEG./CM

R. F. BORESIGHT POSITION

+0.5°

S.T. — 2 SEC.
O.S. — 52 %

—0—

NORMAL TYPE II SYSTEM

+0.5°

S.T. — 4 SEC.
O.S. — 40 %

LOW GAIN TYPE II SYSTEM

+0.5°

S.T. — 2 SEC.
O.S.— 25 %

—0—

**LOW GAIN TYPE II SYSTEM
WITH EBS**

Figure 10—System Response to a
Position Step Input

36
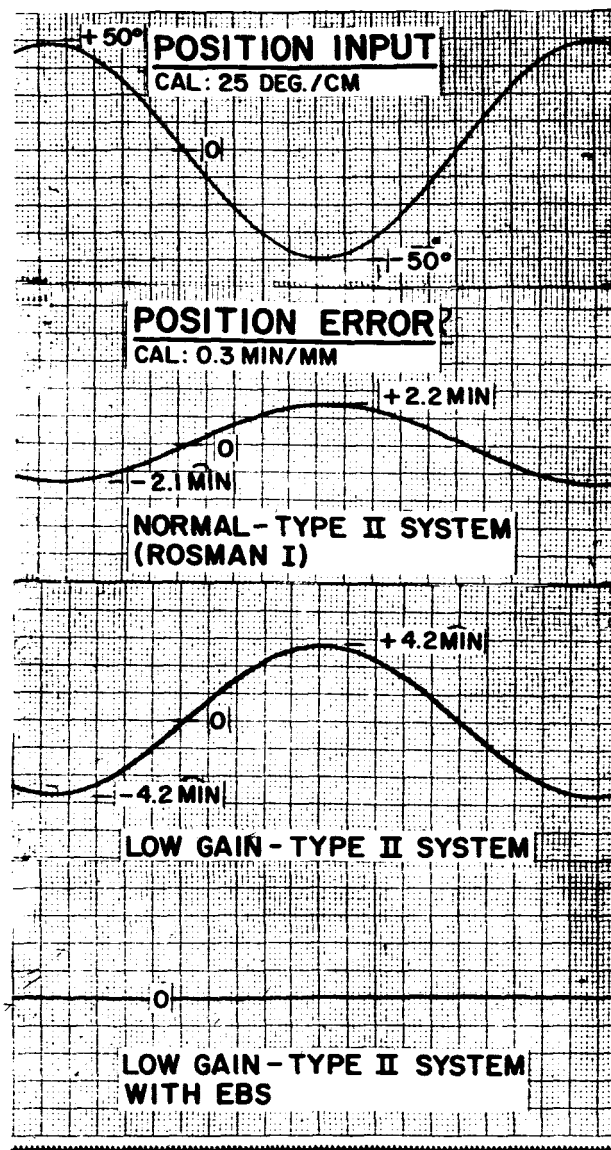
Figure 11—System Response to a 0.01 CPS Sine
Wave Input
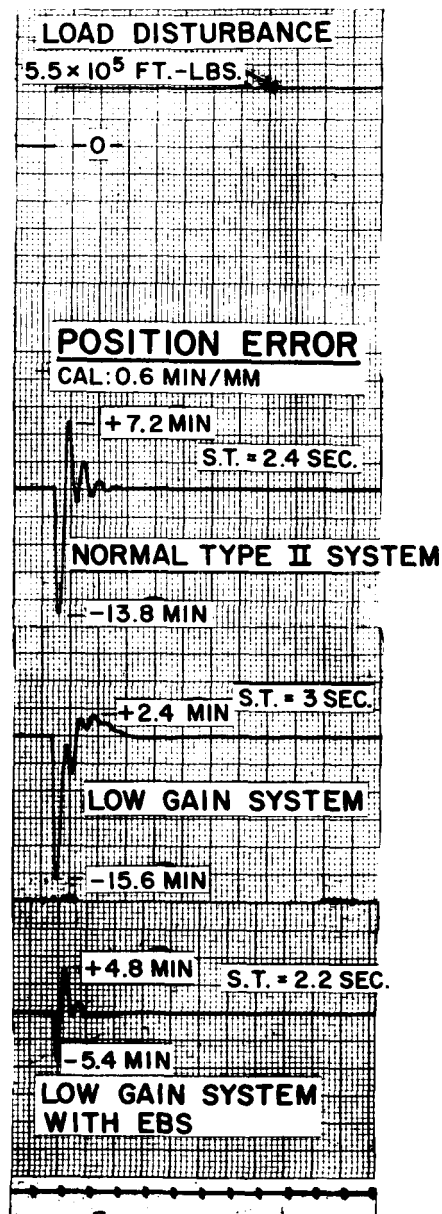
Figure 12—System Response to
a Load Disturbance

38

CIRCULAR APERTURE CALCULATIONS

Following the development for the rectangular aperture of dimension a, b in Reference [3], p. 180, the expression

$$g(\theta, \varphi) = \int_{-a/2}^{+a/2} \int_{-b/2}^{+b/2} F(\zeta,\eta)\,e^{jk\,\sin\theta(\zeta\,\cos\varphi + \eta\,\sin\varphi)}\,d\zeta\,d\eta.$$

goes over to

$$g(\theta, \varphi) = \int_{\varphi'=0}^{2\pi} \int_{r'=0}^{a} F(r', \varphi')\,e^{jk\,\sin\theta\,(r'\cos\varphi'\,\cos\varphi + r'\,\sin\varphi'\sin\varphi)}\,r'\,dr'\,d\varphi'$$

for the circular aperture if a = radius, k = $2\pi/\lambda$, and r'dφ'dr'= differential area on the aperture.   Then

$$g(\theta, \varphi) = \int_{\varphi'=0}^{2\pi} \int_{r'=0}^{a} F(r', \varphi')\,e^{jkr'\sin\theta\cos(\varphi-\varphi')}\,r'\,dr'\,d\varphi'$$

If $\rho = r'/a$, u = $\dfrac{2\pi a \sin\theta}{\lambda}$, and F(r', φ') = F(r') only,

$$g(u, \varphi) = a^2 \int_{\varphi'=0}^{2\pi} \left[\int_{\rho=0}^{1} F(\rho)\,\rho\,d\rho \right] e^{j\,u\rho\,\cos(\varphi-\varphi')}\,d\varphi'$$
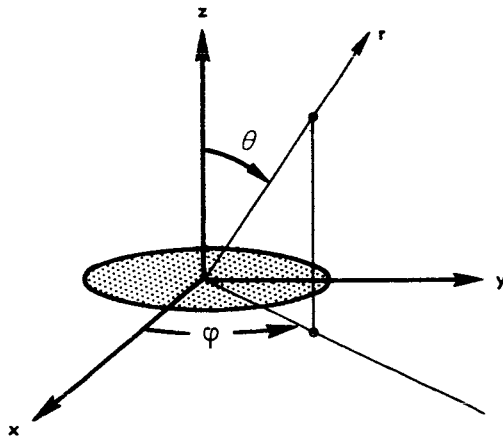

Figure 13—Circular Aperture Coordinates

For approximately cosinusoidal amplitude illumination with uniform phase distribution,

$$F(\rho) = \cos\left(\frac{\pi\,\rho}{2}\right) \cong (1 - \rho^2).$$

Therefore, since

$$\int_0^{2\pi} e^{jur\cos(\varphi-\varphi')}\,d\varphi' = 2\pi\,J_0(ur),$$

$$g(u, \varphi) = 2\pi\,a^2 \int_{\rho=0}^1 (1 - \rho^2)\rho\,[J_0(u\rho)]\,d\rho.$$

From Ref. [13], p. 163

$$J_{p-1}(\alpha x) + J_{p+1}(\alpha x) = \frac{2p}{\alpha x}\,J_p(\alpha x).$$

It follows, upon setting $p = 1$, $\alpha = u$, and $x = \rho$ that

$$\frac{g(u, \varphi)}{2\pi\,a^2} = \int_{\rho=0}^1 \rho\,J_0(u\rho)\,d\rho - \int_{\rho=0}^1 \rho^3\,J_0(u\rho)\,d\rho$$

$$= \int_{\rho=0}^1 \rho\,J_0(u\rho)\,d\rho + \int_{\rho=0}^1 \rho^3\,J_2(u\rho)\,d\rho - \frac{2}{u}\int_{\rho=0}^1 \rho^2\,J_1(u\rho)\,d\rho.$$

Again, from Ref. [13], p. 162

$$\frac{d}{dx}\,[x^p\,J_p\,(\alpha x)] = \alpha x^p\,J_{p-1}(\alpha x).$$

40

Upon setting $p = 1$, $p = 2$, $p = 3$ successively in the above,

$$\frac{g(u, \varphi)}{2\pi a^2} = \frac{\rho}{u} J_1(u\rho) \Big|_0^1 + \frac{\rho^3}{u} J_3(u\rho) \Big|_0^1 - 2 \frac{\rho^2}{u^2} J_2(u\rho) \Big|_0^1$$

$$= \frac{1}{u} (J_1(u) + J_3(u)) - \frac{2}{u^2} J_2(u)$$

$$= \frac{2}{u^2} J_2(u)$$

Since $J_N(u) = \frac{(u/2)^N}{N!} \Lambda_N(u)$, Ref. [14], p. 128;

for $N = 2$, $J_2(u) = \frac{u^2}{8} \Lambda_2(u)$, and

$$g(u, \varphi) = g(u) = \frac{\pi a^2}{2} \Lambda_2(u).$$

By normalizing the above, the two radiation pattern functions which are to be compared are

$$f(u) = \frac{(\pi^2/4) \cos u}{(\pi^2/4 - u^3)} \quad \text{and}$$

$g(u) = \Lambda_2(u)$, which are shown in Figure 14.

1.0

0.8

-3 db

0.6
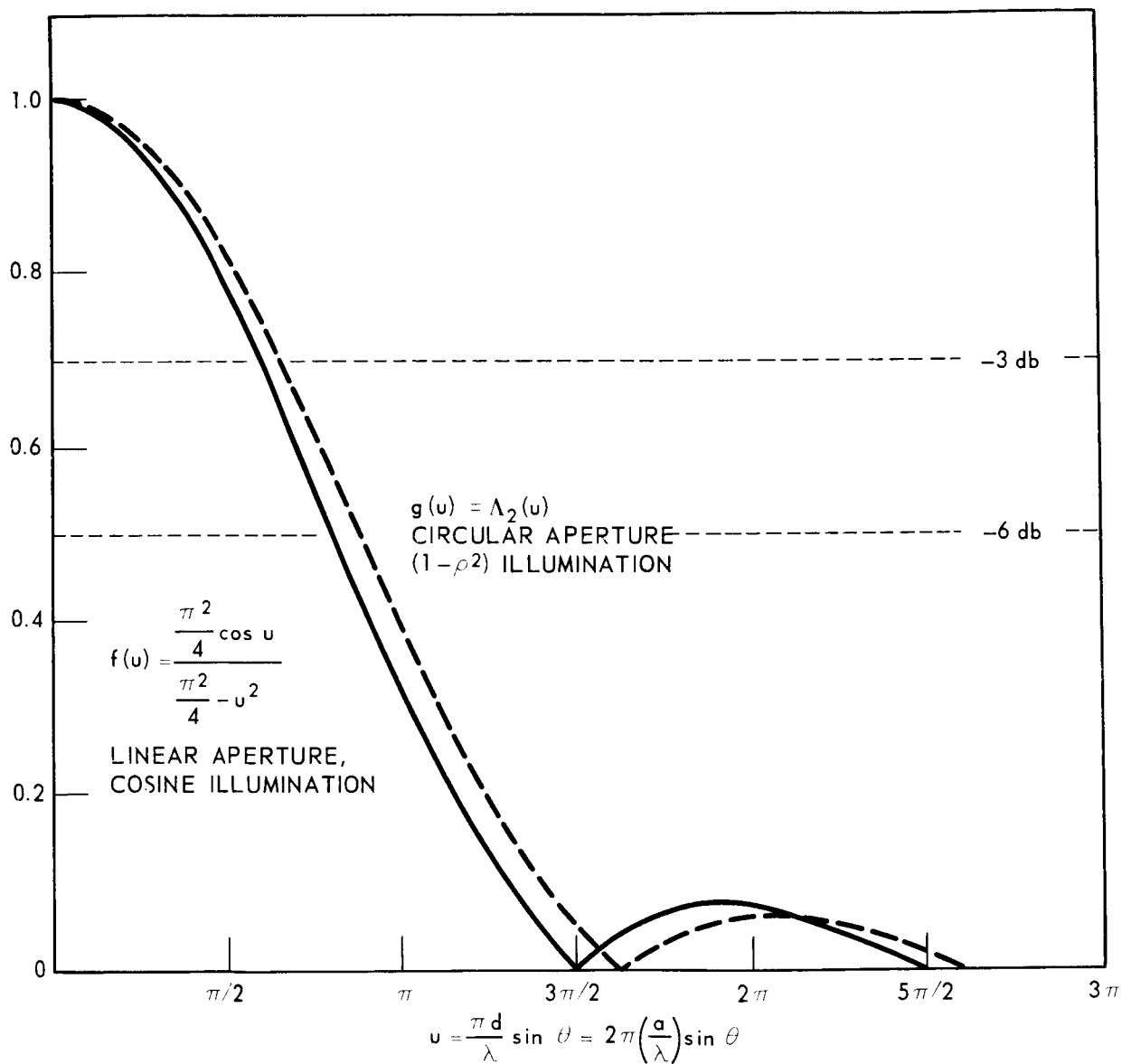
$g(u) = \Lambda_2(u)$
CIRCULAR APERTURE
$(1-\rho^2)$ ILLUMINATION
-6 db

0.4

$$f(u) = \frac{\dfrac{\pi^2}{4}\cos u}{\dfrac{\pi^2}{4} - u^2}$$

LINEAR APERTURE,
COSINE ILLUMINATION

0.2

0

$\pi/2$ π $3\pi/2$ 2π $5\pi/2$ 3π

$$u = \frac{\pi d}{\lambda}\sin\,\theta = 2\pi\left(\frac{a}{\lambda}\right)\sin\,\theta$$

Figure 14—Comparison of Radiation Pattern Functions

$$f(u)\frac{\dfrac{\pi^2}{4}\cos u}{\dfrac{\pi^2}{4} - u^2} \quad \text{and} \quad g(u) = \Lambda_2(u)$$

42

APPENDIX III
GENERATION OF SECONDARY PATTERNS
FOR THE DUAL PLANE CASE

$$\overline{x}' = A\,\overline{x}$$

$$
\begin{bmatrix} x' \\ y' \\ z' \end{bmatrix} =
\begin{bmatrix} A_{11} & A_{12} & A_{13} \\ A_{21} & A_{22} & A_{23} \\ A_{31} & A_{32} & A_{33} \end{bmatrix}
\begin{bmatrix} x \\ y \\ z \end{bmatrix}
$$

Figure 15—Feeds and Beams

$x = r \sin \theta \cos \varphi$ $x' = r \sin \theta' \cos \varphi'$

$y = r \sin \theta \sin \varphi$ $y' = r \sin \theta' \sin \varphi'$

$z = r \cos \theta$ $z' = r \cos \theta'$

$$
A = \begin{bmatrix}
(\cos \gamma \cos \alpha - \cos \beta \sin \alpha \sin \gamma) & (\cos \gamma \sin \alpha + \cos \beta \cos \alpha \sin \gamma) & (\sin \gamma \sin \beta) \\
(-\sin \gamma \cos \alpha - \cos \beta \sin \alpha \cos \gamma) & (-\sin \gamma \sin \alpha + \cos \beta \cos \alpha \cos \gamma) & (\cos \gamma \sin \beta) \\
(\sin \beta \sin \alpha) & (-\sin \beta \cos \alpha) & (\cos \beta)
\end{bmatrix}
$$

Euler angles

α determined by feed positions.

β equal to squint angle θ_s.

γ equal to zero due to assumed rotational symmetry of beams.
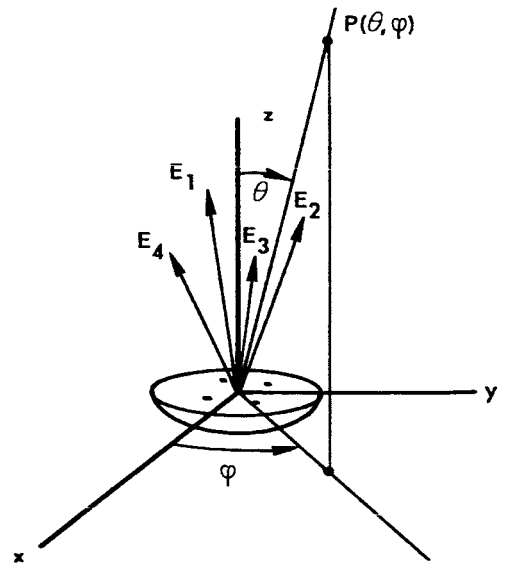
Figure 16—Coordinate Conventions ⟶

43

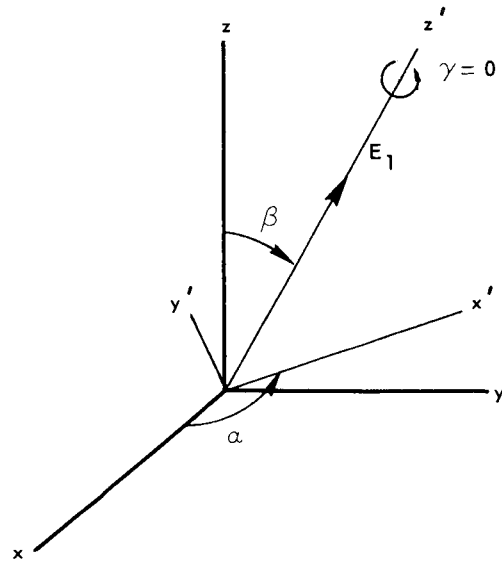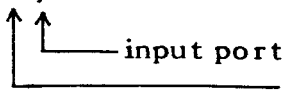| Freq. f	136 Mc.	400 Mc.	1705 Mc.
diam (d)	11.75λ	34.57λ	147.3λ
squint (θ_s)	$3.61°$	$1.22°$	$0.284°$
a_1	$315°$	$315°$	$315°$
a_2	$225°$	$225°$	$225°$
a_3	$135°$	$135°$	$135°$
a_4	$45°$	$45°$	$45°$

Figure 17—Euler Angles

$$\sin\theta' \cos\varphi' = A_{11} \sin\theta \cos\varphi + A_{12} \sin\theta \sin\varphi + A_{13} \cos\theta$$

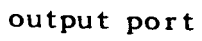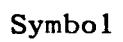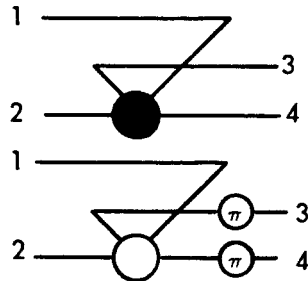$$\sin\theta' \sin\varphi' = A_{21} \sin\theta \cos\varphi + A_{22} \sin\theta \sin\varphi + A_{23} \cos\theta$$

$$\cos\theta' = A_{31} \sin\theta \cos\varphi + A_{32} \sin\theta \sin\varphi + A_{33} \cos\theta$$

$$E_1 = \frac{\cos u}{\dfrac{\pi^2}{4} - u^2}, \quad u = \frac{\pi d}{\lambda} \sin\theta'; \quad E_1 \Rightarrow \theta^{I}, \; E_2 \Rightarrow \theta^{II}, \; E_3 \Rightarrow \theta^{III}, \; E_4 \Rightarrow \theta^{IV}.$$

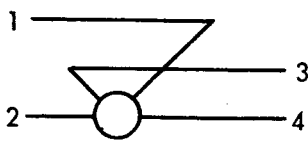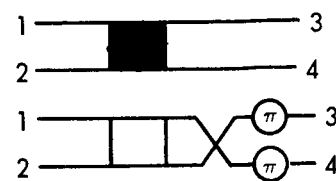# SCATTERING AND TRANSFER MATRIX FORMS IN V_4 (c)

$i \Rightarrow$ row, $j \Rightarrow$ column

S_{ij} T_{ij} Symbol

input port

output port

$$\bullet S_{ij} = \frac{j}{\sqrt{2}} \begin{bmatrix} 0 & 0 & | & 1 & 1 \\ & & | & & \\ 0 & 0 & | & 1 & -1 \\ - & - & - & - & - \\ 1 & 1 & | & 0 & 0 \\ & & | & & \\ 1 & -1 & | & 0 & 0 \end{bmatrix}$$

$$\bullet T_{ij} = \frac{j}{\sqrt{2}} \begin{bmatrix} 1 & 0 & | & 1 & 0 \\ & & | & & \\ 0 & -1 & | & 0 & -1 \\ - & - & - & - & - \\ 1 & 0 & | & -1 & 0 \\ & & | & & \\ 0 & -1 & | & 0 & 1 \end{bmatrix}$$

(a)

$$_\circ S_{ij} = \frac{-j}{\sqrt{2}} \begin{bmatrix} 0 & 0 & | & 1 & 1 \\ & & | & & \\ 0 & 0 & | & 1 & -1 \\ - & - & - & - & - \\ 1 & 1 & | & 0 & 0 \\ & & | & & \\ 1 & -1 & | & 0 & 0 \end{bmatrix}$$

$$_\circ T_{ij} = \frac{j}{\sqrt{2}} \begin{bmatrix} -1 & 0 & | & -1 & 0 \\ & & | & & \\ 0 & 1 & | & 0 & -1 \\ - & - & - & - & - \\ -1 & 0 & | & 1 & 0 \\ & & | & & \\ 0 & -1 & | & 0 & -1 \end{bmatrix}$$

(b)

45

S_{ij} ⬛ T_{ij} ⬛ Symbol

$$\blacksquare S_{ij} = \frac{1}{\sqrt{2}} \begin{bmatrix} 0 & 0 & | & 1 & j \\ & & | & & \\ 0 & 0 & | & j & 1 \\ - & - & - & - & - \\ 1 & j & | & 0 & 0 \\ & & | & & \\ j & 1 & | & 0 & 0 \end{bmatrix}$$

$$\blacksquare T_{ij} = \frac{1}{\sqrt{2}} \begin{bmatrix} 1 & 0 & | & j & 0 \\ & & | & & \\ 0 & 1 & | & 0 & -j \\ - & - & - & - & - \\ j & 0 & | & 1 & 0 \\ & & | & & \\ 0 & -j & | & 0 & 1 \end{bmatrix}$$

(c)

$$\square S_{ij} = \frac{-1}{\sqrt{2}} \begin{bmatrix} 0 & 0 & | & j & 1 \\ & & | & & \\ 0 & 0 & | & 1 & j \\ - & - & - & - & - \\ j & 1 & | & 0 & 0 \\ & & | & & \\ 1 & j & | & 0 & 0 \end{bmatrix}$$

$$\square T_{ij} = \frac{1}{\sqrt{2}} \begin{bmatrix} -j & 0 & | & -1 & 0 \\ & & | & & \\ 0 & j & | & 0 & -1 \\ - & - & - & - & - \\ -1 & 0 & | & -j & 0 \\ & & | & & \\ 0 & -1 & | & 0 & j \end{bmatrix}$$

(d)

$$_\beta S_{ij} = \begin{bmatrix} 0 & 0 & | & e^{-j\psi_1} & 0 \\ & & | & & \\ 0 & 0 & | & 0 & e^{-j\psi_2} \\ - & - & - & - & - \\ e^{-j\psi_1} & 0 & | & 0 & 0 \\ & & | & & \\ 0 & e^{-j\psi_2} & | & 0 & 0 \end{bmatrix}$$

$$_\beta T_{ij} = \begin{bmatrix} e^{-j\psi_1} & 0 & | & 0 & 0 \\ & & | & & \\ 0 & e^{j\psi_1} & | & 0 & 0 \\ - & - & - & - & - \\ 0 & 0 & | & e^{-j\psi_2} & 0 \\ & & | & & \\ 0 & 0 & | & 0 & e^{j\psi_2} \end{bmatrix}$$

(e)
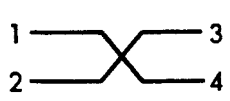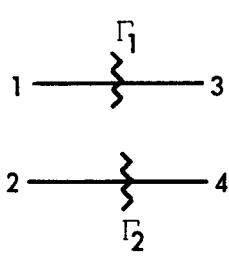
$$S_{ij} \qquad\qquad T_{ij} \qquad\qquad \text{Symbol}$$

$$_\sigma S_{ij} = \begin{bmatrix} 0 & 0 & 0 & 1 \\ 0 & 0 & 1 & 0 \\ 0 & 1 & 0 & 0 \\ 1 & 0 & 0 & 0 \end{bmatrix} \qquad _\sigma T_{ij} = \begin{bmatrix} 0 & 0 & 1 & 0 \\ 0 & 0 & 0 & 1 \\ 1 & 0 & 0 & 0 \\ 0 & 1 & 0 & 0 \end{bmatrix}$$

(f)

$$_\Gamma S_{ij} = \begin{bmatrix} 0 & 0 & \Gamma_1 & 0 \\ 0 & 0 & 0 & \Gamma_2 \\ \Gamma_1 & 0 & 0 & 0 \\ 0 & \Gamma_2 & 0 & 0 \end{bmatrix} \qquad _\Gamma T_{ij} = \begin{bmatrix} \Gamma_1 & 0 & 0 & 0 \\ 0 & \Gamma_1^{-1} & 0 & 0 \\ 0 & 0 & \Gamma_2 & 0 \\ 0 & 0 & 0 & \Gamma_2^{-1} \end{bmatrix}$$

(g)

Figure 18—Scattering and Transfer Matrices

DERIVATION OF TRANSFER MATRIX FROM SCATTERING MATRIX IN V_4 (c)

Given that

$$\bullet S_{ij} = \frac{j}{\sqrt{2}} \begin{bmatrix} 0 & 0 & | & 1 & 1 \\ & & | & & \\ 0 & 0 & | & 1 & -1 \\ - & - & - & - & - \\ 1 & 1 & | & 0 & 0 \\ & & | & & \\ 1 & -1 & | & 0 & 0 \end{bmatrix} = \begin{bmatrix} S_{11} & S_{12} & | & S_{13} & S_{14} \\ & & | & & \\ S_{21} & S_{22} & | & S_{23} & S_{24} \\ - & - & - & - & - \\ S_{31} & S_{32} & | & S_{33} & S_{34} \\ & & | & & \\ S_{41} & S_{42} & | & S_{43} & S_{44} \end{bmatrix}$$

$$\overline{b} = S \, \overline{a}$$

$$\begin{bmatrix} b_1 \\ b_2 \\ b_3 \\ b_4 \end{bmatrix} = \bullet S_{ij} \begin{bmatrix} a_1 \\ a_2 \\ a_3 \\ a_4 \end{bmatrix}$$

h_1 , a_1 $\longrightarrow$ $\qquad$ $\longrightarrow$ b_3 , g_1

h_2 , b_1 $\longleftarrow$ $\qquad$ 3 $\longleftarrow$ a_3 , g_2

h_3 , a_2 $\longrightarrow$ $\qquad$ $\longrightarrow$ b_4 , g_3

h_4 , b_2 $\longleftarrow$ $\qquad$ $\longleftarrow$ a_4 , g_4
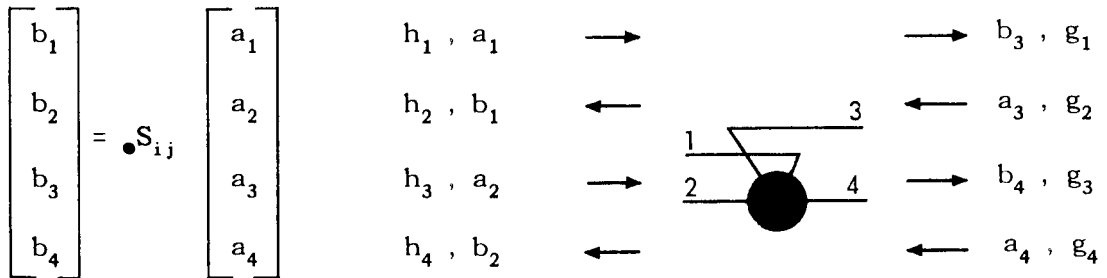

Figure 19—Terminal Conventions

$$\frac{\sqrt{2}}{j} \, b_1 = S_{11} \, a_1 + S_{12} \, a_2 + S_{13} \, a_3 + S_{14} \, a_4 \qquad (1)$$

$$\frac{\sqrt{2}}{j} \, b_2 = S_{21} \, a_1 + S_{22} \, a_2 + S_{23} \, a_3 + S_{24} \, a_4 \qquad (2)$$

$$\frac{\sqrt{2}}{j} \, b_3 = S_{31} \, a_1 + S_{32} \, a_2 + S_{33} \, a_3 + S_{34} \, a_4 \qquad (3)$$

$$\frac{\sqrt{2}}{j} \, b_4 = S_{41} \, a_1 + S_{42} \, a_2 + S_{43} \, a_3 + S_{44} \, a_4 \qquad (4)$$

$$\bar{g} = T \, \bar{h}$$

$$\begin{bmatrix} g_1 \\ g_2 \\ g_3 \\ g_4 \end{bmatrix} = {}_{\bullet}T_{ij} \begin{bmatrix} h_1 \\ h_2 \\ h_3 \\ h_4 \end{bmatrix} \qquad {}_{\bullet}T_{ij} = \begin{bmatrix} T_{11} & T_{12} & | & T_{13} & T_{14} \\ & & | & & \\ T_{21} & T_{22} & | & T_{23} & T_{24} \\ - & - & - & - & - & - & - \\ T_{31} & T_{32} & | & T_{33} & T_{34} \\ & & | & & \\ T_{41} & T_{42} & | & T_{43} & T_{44} \end{bmatrix}$$

$$g_1 = T_{11} \, h_1 + T_{12} \, h_2 + T_{13} \, h_3 + T_{14} \, h_4 \qquad (5)$$

$$g_2 = T_{21} \, h_1 + T_{22} \, h_2 + T_{23} \, h_3 + T_{24} \, h_4 \qquad (6)$$

$$g_3 = T_{31} \, h_1 + T_{32} \, h_2 + T_{33} \, h_3 + T_{34} \, h_4 \qquad (7)$$

$$g_4 = T_{41} \, h_1 + T_{42} \, h_2 + T_{43} \, h_3 + T_{44} \, h_4 \qquad (8)$$

Solving equations (3) and (5) for g_1 :

$$S_{31} \, h_1 + S_{32} \, h_3 + S_{33} \, g_2 + S_{34} \, g_4 = (T_{11} \, h_1 + T_{12} \, h_2 + T_{13} \, h_3 + T_{14} \, h_4) \, \frac{\sqrt{2}}{j}$$

Solving equations (4) and (7) for g_3 :

$$S_{41} \, h_1 + S_{42} \, h_3 + S_{43} \, g_2 + S_{44} \, g_4 = (T_{31} \, h_1 + T_{32} \, h_2 + T_{33} \, h_3 + T_{34} \, h_4) \, \frac{\sqrt{2}}{j}$$

Therefore $\qquad T_{12} = T_{14} = T_{32} = T_{34} = 0$

$$T_{11} = S_{31}(j/\sqrt{2}) \; = \; (j/\sqrt{2}) = T_{13} = T_{31}$$

$$T_{33} = S_{42}(j/\sqrt{2}) = -\,(j/\sqrt{2})$$

Solving equations (1) and (2) for g_2 and g_4 :

$$\frac{\sqrt{2}}{j} h_2 - S_{11} h_1 - S_{12} h_3 = S_{13} g_2 + S_{14} g_4$$

$$\frac{\sqrt{2}}{j} h_4 - S_{21} h_1 - S_{22} h_3 = S_{23} g_2 + S_{24} g_4$$

It follows that

$$g_2 = \frac{\sqrt{2}}{j} \left(\frac{h_2}{S_{14}} - \frac{h_4}{S_{24}} \right) \Big/ \left(\frac{S_{13}}{S_{14}} - \frac{S_{23}}{S_{24}} \right) = T_{21} h_1 + T_{22} h_2 + T_{23} h_3 + T_{24} h_4$$

$$g_4 = \frac{\sqrt{2}}{j} \left(\frac{h_2}{S_{13}} - \frac{h_4}{S_{23}} \right) \Big/ \left(\frac{S_{14}}{S_{13}} - \frac{S_{24}}{S_{23}} \right) = T_{41} h_1 + T_{42} h_2 + T_{43} h_3 + T_{44} h_4$$

Therefore

$$T_{21} = T_{23} = T_{41} = T_{43} = 0$$

$$T_{22} = T_{24} = T_{42} = (- j / \sqrt{2})$$

$$T_{44} = (j / \sqrt{2})$$

Then

$$\bullet T_j = \frac{j}{\sqrt{2}} \begin{bmatrix} 1 & 0 & | & 1 & 0 \\ & & | & & \\ 0 & -1 & | & 0 & -1 \\ -- & -- & -- & -- & -- \\ 1 & 0 & | & -1 & 0 \\ & & | & & \\ 0 & -1 & | & 0 & 1 \end{bmatrix}$$

50

ACKNOWLEDGMENTS

REFERENCES

[1] Stephenson, J.M., et al, "Design Criteria for a Large Multipurpose Tracking Antenna," Philco Corporation, Western Development Laboratories, Contract AF 04(647)-532, WOL Tech. Rpt. 1368 Appendix D

[2] Rhodes, D.R., Ph.D., "Introduction to Monopulse," McGraw-Hill, 1959

[3] Silver, S., "Microwave Antenna Theory and Design," McGraw-Hill, 1949

[4] Goldstein, H., Ph.D., "Classical Mechanics," Addison-Wesley, 1959

[5] Smirnov, V., "Linear Algebra and Group Theory," McGraw-Hill, 1961

[6] Lax, B., Ph.D., Button, K., "Microwave Ferrites and Ferrimagnetics," McGraw-Hill, 1962

[7] Montgomery, C., Dicke, R., Purcell, E., "Principles of Microwave Circuits," McGraw-Hill, 1948

[8] Paige, L., Swift, J., "Linear Algebra," Ginn, 1961

[9] Youla, D., Kaplan, L., Stock, D., "The Analytic Foundations of Linear Time-Invariant N-Ports," Contract No. AF-19(604)-4143, 1962

[10] Carlin, H., Giordano, A., "Network Theory," Prentice-Hall, 1964

[11] Mal'cev, A., "Foundations of Linear Algebra," Freeman, 1963

[12] Stoll, R., "Linear Algebra and Matrix Theory," McGraw-Hill, 1952

[13] Hildebrand, F., "Advanced Calculus for Engineers," Prentice-Hall, 1949

[14] Jahnke, E. and Emde, F., "Tables of Functions," Dover, 1945